UNIVERSITÀ DEGLI STUDI DI PADOVA

Dipartimento di Fisica e Astronomia "Galileo Galilei"

Corso di Laurea Magistrale in Fisica

Tesi di Laurea

Controlling foam ageing in viscoelastic media

Relatore

Prof. Giampaolo Mistura

Correlatrici

Prof. Anniina Salonen

Prof. Emmanuelle Rio

Laureanda

Chiara Guidolin

Anno Accademico 2017/2018

Per aspera ad astra

Acknowledgements

The present thesis is the result of the internship done at LPS laboratory of Université Paris-Sud in Orsay, France.

First of all, I would like to express my gratitude to my supervisor Prof. Anniina Salonen for taking me into MMOI research group and giving me the opportunity to discover the wonderful world of foams. I can not find the right words to thank her for constantly supporting me with her contagious enthusiasm.

I would like to thank Prof. Emmanuelle Rio as well, for being always ready to kindly help me and especially for the patience she showed in teaching me how to deal with Matlab struggles. I am also grateful to all the people of MMOI group for making me always feel welcome during my stay.

I would like to thank Prof. Giampaolo Mistura, for accepting to be my internal supervisor and for providing me precious advice which made me understand what I really want to do after my master degree.

A great thank goes to my mother and my brother, for always leaving me free to decide about my education. We are the only ones who know the sacrifice we did and what this degree means to us. I think I will never thank them enough.

I owe the most special thank to Tommaso, for his love and his unconditional support, for always trusting me and pushing me to do my best even when I was not sure I could do it. I would have never reached this goal without him by my side.

Finally, I thank myself for my tenacity and determination, which allowed me to never give up despite all the countless adversities.

Contents

Introduction

A foam can be roughly defined as a dispersion of gas bubbles in a continuous medium. Everyone meets several kinds of foams in daily life, from whipped-cream to sea "white horses", from shampoo lather to the head on a pint of beer.

Each foam contains stabilisers, such as surface active molecules, polymers or particles, which make the bubbles stable by arranging themselves at the gas/liquid interfaces.

This complex system is characterised by a typical cellular structure. The gas bubbles are tightly packed together, so that the liquid phase is spread in a network of thin films between neighbouring bubbles, and Plateau borders, that are triangular-shaped channels made by the intersection of three different films [18].

Thanks to their lightness, their large surface area and their peculiar mechanical properties [19], foams often represent the best solution for a large number of industrial applications [6]. Liquid foams are usually preferable to other fluids because they allow to employ less material, by filling the same volume without decreasing the product effect. Treating a material with a foam rather than a liquid, leads not only to a product economy but also to a much less waste to reprocess afterwards. This aspect finds application, for example, in the decontamination of nuclear power stations and in all those processes which require a capture of small solid particles, ions or molecules. Furthermore, the large number of interfaces inside a foam increases enormously the possibilities for molecular transfer, which has relevance in food industry, where foams are used as strong flavour enhancers, allowing to reduce salt and sugar contents [9]. Foams ability to quickly fill large spaces makes them suitable also for fire-fighting, since they rapidly smother the fire by isolating the source of combustion from oxygen in the air. Finally, liquid foams are employed as precursors in the production of solid foams for industrial purposes, such as polyurethane and cellular concrete, but also for our daily life, such as bread, cakes and meringues.

Foams are intrinsically unstable. During their life, they can undergo three different mechanisms of destabilisation: drainage, coalescence and coarsening. Drainage is due to the flow of the liquid through the Plateau borders, driven by gravity, and results in a dryer foam on the top and a wetter foam on the bottom. Coalescence consists of the thinning and consequent rupture of the film between neighbouring bubbles. Finally, coarsening is due to the gas flux between bubbles of different size, driven by the Laplace pressure difference.

These ageing processes alter the foam structure and can be a strong limitation, for example, to the elaboration of solid foams with a controlled morphology, inherited from their liquid precursors. Since the final solid foam structure depends on the ageing processes occured during solidification, stable liquid precursors where ageing is slowed down or arrested are crucial to design materials with controlled bubble size, gas volume fraction and packing structure.

The desired longevity of a foam is then clearly related to the specific applications, which call for a thorough understanding of foam stabilisation. This explains the increasing interest in studying the origins of foam ageing mechanisms and the different possibilities to inhibit them.

Several strategies to obtain highly stable foams have been reported in the scientific literature. The rate of gravitational drainage can be decreased by increasing the viscosity of the continuous phase. For this purpose, several studies report the use of complex fluids such as clay particles [17] or flocculated suspensions [23]. Recently, experimental studies have been developed in foams where the aqueous phase consists of a polymer hydrogel [8]. When the foam is not too dry, coalescence can be in principle avoided if the surface active molecules are efficient enough to withstand film rupture. Finally, it has been observed that the coarsening process can be slowed down either if an insoluble gas is used to form bubbles or if the continuous phase is made of polymer gels [3].

The purpose of the present thesis is to investigate how the mechanical properties of the continuous phase impact on foam coarsening, in conditions where drainage and coalescence can both be neglected. In order to do that, we shall use emulsions as liquid phase, because of their viscoelasticity, which will be first investigated by rheological measurements. It will be a preliminary experimental study, since there is a lack of fundamental studies devoted to foamed emulsions stability.

Traditional microscopy is not suitable for probing the internal structure of three dimensional foams, because the high number of interfaces scatter light. Moreover, the study of foams requires the application of non-invasive methods: treatments like dilution, freezing or drying would result in fact in an irreversible sample damage.

Thus, foamed emulsions will be studied by employing diffusing-wave spectroscopy, a technique which exploits the strong multiple scattering undergone by transmitted light to get information about the average bubble size and their rearrangements during coarsening. Finally, quasi-2D foam imaging experiments will be carried out in order to estimate the gas permeability of the liquid films between the bubbles.

The present thesis is organised as follows. In the first chapter a theoretical overview of the foam systems will be presented. We shall first describe the structure of foams at equilibrium and then explain the main mechanisms of foam ageing, focussing on foam coarsening either in two or three dimensions. In the second chapter all the experimental methods employed will be illustrated in detail. Finally, in the third chapter we shall report and analyse all the results obtained.

1 Theoretical background

In this chapter, we shall present the scientific background for the basic understanding of foam systems. We will start from a short description of foam structure at equilibrium. Before speaking about the different mechanisms of liquid foam destabilization, we will explain the relevant role of surfactants in foam stability. We will then highlight the main aspects of foam coarsening, from theoretical prediction to experimental observations in the literature. Finally, we shall explain how to study coarsening without the effects of drainage and coalescence, showing the relevance of the mechanical properties of the liquid phase and justifying our choice to study foamed emulsions.

1.1 Foam structure at equilibrium

Foams are multiscale systems, since they present peculiar structures on different length scales, ranging from macroscopic to molecular.

At the observer's scale, a liquid foam appears as a soft, opaque and homogeneous solid, as shown in figure 1.1 (a). At this macroscopic level its exterior aspect and properties may be totally characterised by its *liquid volume fraction*, defined as:

$$\epsilon = \frac{V_{liq}}{V_{foam}} \tag{1.1}$$

that is the ratio between the volume of liquid V_{liq} and the total volume of the foam V_{foam}, which quantifies the amount of liquid contained in it.

A jump into a millimetric scale shows something more about the structure: as can be seen in figure 1.1 (b), foams are metastable packings of small soft units, gas bubbles, whose typical size ranges from 10 μm to 1 cm.

Depending on the liquid fraction, this cellular structure may appear very different. If ϵ is higher than a critical value ϵ^*, the bubbles are spherical and do not touch each other: this is what is called a *bubbly liquid*. When $\epsilon < \epsilon^*$ the bubbles start touching each other and change their shape into squashed spheres: this is a *wet foam*. Further decreasing the liquid fraction, the bubbles start to be polyhedral, giving rise to a *dry foam*. The transition from bubbly liquid to wet foam occurs at a precise value of liquid fraction ϵ^* close to 0.36, corresponding to the vanishing of the osmotic pressure.

By contrast, the transition between wet and dry foam is less well defined: we usually speak of dry foam when the presence of the liquid plays a negligible role in the observed phenomenon, typically when $\epsilon < 5\%$ [6].

A closer look reveals how the liquid is distributed among the bubbles. Let us first consider a foam whose liquid fraction is sufficiently small. Here, a foam can be thought of as a network of thin liquid films that separate neighbouring bubbles, with a thickness generally between 10 nm and a few μm. Three films intersect along the edges, forming liquid-carrying channels named *Plateau borders* after Joseph Plateau (1801 - 1883). They act as collectors of liquid coming from the films and they have a triangle-shaped cross section with concave sides, as sketched in figure 1.1 (c). Then four Plateau borders meet in a junction that is called *vertex* or *node*.

The structure of a real foam is not completely disordered: a small group of local geometric rules, named Plateau's laws, describes how the bubbles pack together to form the foam skeleton. In a three-dimensional dry foam the bubble shape is approximately polyhedral and those rules state that, at equilibrium, three films must join at each Plateau border at mutual angles of 120^o, resulting from the balancing of the surface tension forces along each film. Likewise, four Plateau borders must form tetrahedral symmetric vertices, with angles of 109.47^o between each other. These angular constraints are satisfied if the polyhedral bubbles have curved faces and edges [22]. Similar rules hold also in two dimensions: if the foam is dry enough and approximately monodisperse, the bubbles assume in average an hexagonal shape.

Descending even more into a nanometric scale, the molecular structure of the interfaces appears. The presence of particular molecules, which position themselves at the gas/liquid interfaces like in figure 1.1 (d), is essential to the understanding of the formation and stability of foams, whose specific aspects are better discussed in the next paragraph.

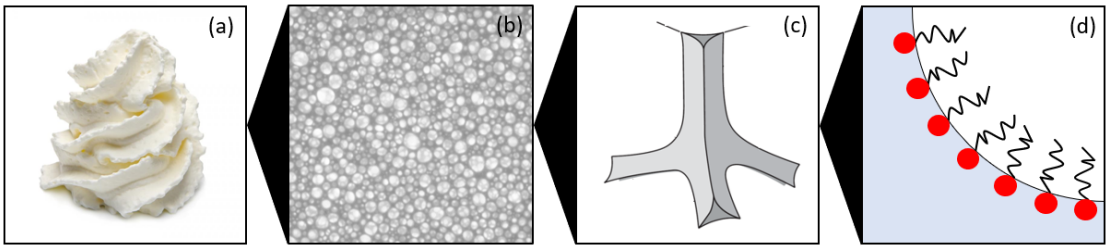

Figure 1.1: **Foam: a multiscale system.** *These pictures show the typical structures displayed by foams at different scales. At the observer's scale ($\sim 10^{-2} - 1$ m) it appears like a soft homogeneous solid (a). At a microscopic scale ($\sim 10^{-4} - 10^{-2}$ m) one can recognise the gas bubbles dispersed in the liquid phase (b) and a closer look ($\sim 10^{-8} - 10^{-4}$m) reveals the liquid distribution among them (c). At a molecular scale ($\sim 10^{-10} - 10^{-8}$m) one can observe the structure of the gas liquid interfaces (d).*

1.2 Foamability and the role of surfactants

Foams do not form spontaneously, because energy is required to disperse gas in a liquid. It can be easily observed that not all liquids foam in the same way. They can show different *foamability*, that is a qualitative measure of their capacity to produce a foam by shaking or by injection of air bubbles [6].

To create a new interface of area dA, an amount of energy equal to $dE = \gamma dA$ is needed, where the proportional factor γ is the *surface tension*, measured in Nm^{-1}, that is the force per unit area that the liquid exerts to reduce the interface.
This proportional relation means that the lower the value of γ, the less expensive in energy is the creation of a new interface, suggesting that a low surface tension should improve foamability. However, a low surface tension alone does not ensure foam stability.

As we said in the previous paragraph, two neighbouring bubbles within a foam share a thin film of liquid that appears as a slightly curved facet: this film plays a fundamental role in the overall stability of the foam. In fact, if the gas/liquid interfaces are clean, this is a very unstable situation. The distance between the two interfaces tends to decrease because of Van der Waals forces; the liquid is drawn from the film into the Plateau borders, so that the film starts thinning until it eventually breaks.

In order to make more stable foams, specific kinds of molecules must be added to the solution: *surfactants*. Surfactants usually consist of molecules with a polar hydrophilic head and a long hydrophobic carbon chain for a tail.

If such molecules are dissolved in the liquid, they tend to adsorb to the interfaces, with their heads in the water and their tails in the air. Thus, both sides of the liquid film between two bubbles will be covered by a monolayer of molecules which lowers the surface tension of the interface. Since certain amphiphilic molecules carry a small electric charge, these two layers repel each other mainly by electrostatic repulsion or steric interaction [2]. The repulsive force can be thought of as an effective pressure inside the film, the *disjoining pressure*, which compensates for the Van der Waals attraction, leading to an enhanced stability of the film.

However, it is the adsorption dynamic that matters, that is the speed with which surfactants completely cover the interface. New bubbles need to be covered with surfactant as quickly as possible, so if the adsorption is too slow, the foamability of the solution will be poor, even if the final value of γ is very low.

Moreover, in order to withstand deformations without rupturing, the thin liquid film between bubbles must be somewhat elastic [34]. When the liquid film undergoes a sudden expansion, the expanded portion of the film has a lower surface concentration of surfactants than other parts because the surface area has increased. This causes a local rise in surface tension which provides resistance to further expansions and, at the same time, produces an immediate contraction of the surface.

Since the surface is coupled by viscous forces to the underlying liquid layers, the contraction of the surface induces liquid flow from the low-tension region to the high-tension region, as shown in figure 1.2. The transport of bulk liquid due to surface tension gradients is called *Marangoni effect*: it re-thickens the thin films and provides a resisting force to counteract film thinning and possible rupture.

This effect only exists until the surfactant adsorption equilibrium is re-established in the film. However, there has to be enough surfactant dissolved near the extended surface region to restore the equilibrium, hence the bulk and the surface surfactant concentrations are crucial parameters.

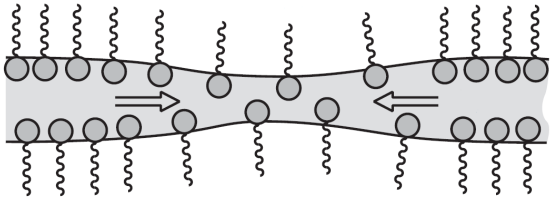

Figure 1.2: **The Marangoni effect.** *The picture sketches the mechanism of liquid mass transfer along the thin film due to the gradient in surface tension. This effect provides stability to the thin film between adjacent bubbles by recovering the film thickness and preventing its rupture.*

Above a certain concentration, called *critical micelle concentration* (*cmc*), surfactants in solution start gathering to form micelles, like the one shown in figure 1.3. Every surfactant has a specific *cmc* which depends on temperature, pressure and on the possible presence of other active molecules. This is an important parameter since before reaching the *cmc*, the surface tension of the solution changes strongly with the surfactant concentration, whereas after reaching the *cmc*, the surface tension remains constant [6].

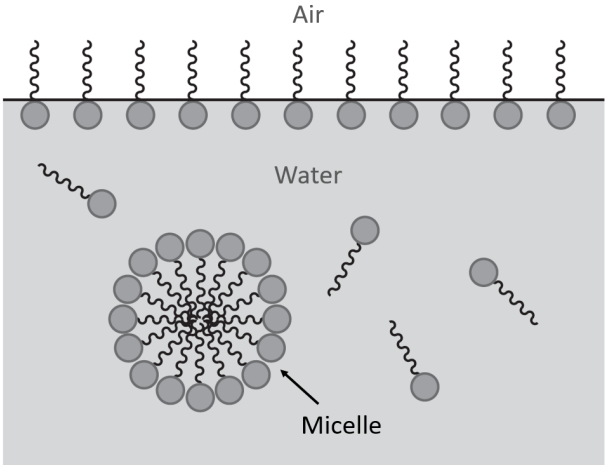

Figure 1.3: **Critical micelle concentration.** *The picture shows the distribution of surfactants at the surface and in the bulk at equilibrium. Above the cmc, surfactants start assembling to form micelles. However, the presence of micelles does not preclude the possibility to find free molecules in solution.*

1.3 Foam ageing

Liquid foams are meta-stable systems. After their generation, they may undergo different mechanisms of destabilisation over time, which slowly lead to a reduction of the total number of bubbles and to a decrease of the foam volume, resulting in an irreversible foam damage. The process that leads the foam to death can be thought of as a competition between three mechanisms: drainage, coalescence and coarsening. The physical reasons which lie behind each of these processes are different, as they impact on foam structure at different scales, but they are strongly correlated to each other. In the next subsections we shall discuss each of these mechanisms separately, with a special focus on foam coarsening, that is the main subject of the present study.

1.3.1 Drainage

Drainage consists of the downward flow of the liquid phase through the foam due to gravity. Since the film thickness is very small at equilibrium, the liquid drainage in dry foams occurs mainly through the network of Plateau borders [21], hence it strongly depends on the cross section of these liquid channels, that is variable and deeply related to the liquid fraction: the wetter the foam, the more pronounced the drainage. Drainage is a crucial process in foam evolution, because it causes a gradual change in the liquid distribution inside the foam. A typical example of drainage effect is shown in figure 1.4. As the liquid flows downwards, the top of the foam becomes dryer than the bottom, the upper bubbles become polyhedral and the Plateau borders become thinner. It is intuitive why it is necessary to find a way to make this effect negligible for studying foam evolution at a constant liquid fraction.

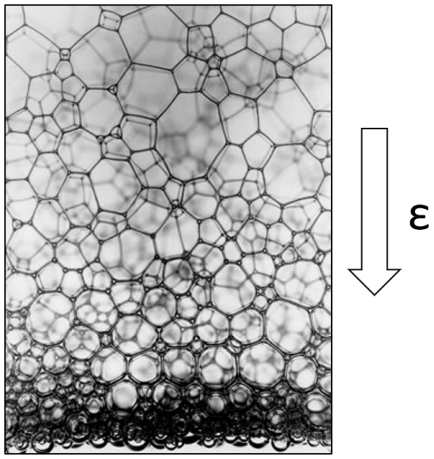

Figure 1.4: **Foam drainage.** *The picture shows a typical example of gravitational drainage in an aqueous foam. As the liquid flows downwards the foam becomes dryer on the top, with polyhedral bubbles, and wetter on the bottom, where the bubbles become approximately spherical.*

1.3.2 Coalescence

When the liquid film between two neighbouring bubbles becomes too thin, it breaks and the bubbles are said to coalesce. This film rupture can occur when the stabilising mechanisms are absent or too weak or it simply results from liquid evaporation when it involves the bubbles on the external part of the foam. This process is strongly coupled to drainage and arises when the liquid fraction decreases below a threshold value depending on the surfactant and its concentration [19]. Despite several hypothesis have been developed to explain its origin [30], coalescence still remains the least understood mechanism of foam evolution. Since two coalescing bubbles give birth to a single final bubble, the essential results of coalescence are a reduction of the total number of bubbles and a loss of gas from the boundary bubbles to the environment, so that the total volume decreases until the foam completely disappears.

1.3.3 Coarsening

If drainage and coalescence are negligible, the main foam ripening mechanism is gas diffusion through the continuous phase, that allows some bubbles to expand at the expense of others, which shrink and gradually disappear. This process is driven by the Laplace pressure difference between two neighbouring bubbles of different sizes, which causes a gas flux from the smaller bubble to the bigger one.

Let us consider a curved surface like the one shown in figure 1.5. The *Young-Laplace law* states that the pressure difference existing between the two sides of the surface is related to the surface tension γ and to the shape of the surface by the two principal radii of curvature R' and R'':

$$\Delta P = P_A - P_B = \gamma \left(\frac{1}{R'} + \frac{1}{R''} \right) \simeq \frac{2\gamma}{R} \qquad if \quad R' \simeq R'' \simeq R \tag{1.2}$$

This relation means that the surface tension tends to reduce the curvature of an interface, making it flatter, and that it is offset by a pressure difference, which tends to bend the interface.

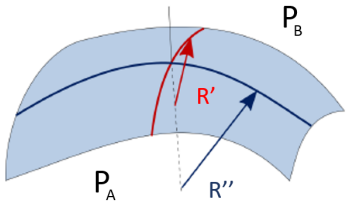

Figure 1.5: **The Young-Laplace law.** *The picture sketches a portion of a curved surface, having principal radii of curvature R' and R''. Pressure is higher in the convex side than in the concave one. The pressure difference between the two sides is proportional to the surface tension and to the surface curvature, according to the Young-Laplace law.*

So if we consider two neighbouring bubbles of different radii R_1 and R_2, the Laplace pressure difference between them will be:

$$\Delta P = 2\gamma \left(\frac{1}{R_1} - \frac{1}{R_2} \right) \tag{1.3}$$

meaning that the bubble with a smaller radius has a higher pressure than the larger one. The fact that large bubbles grow at the expense of smaller ones, leads to a reduction of the total number of bubbles, just like coalescence, but in a completely different way. Once the drainage and coalescence can be neglected, this process leads asymptotically to a scaling behaviour where the bubble growth is statistically self-similar. We shall first present in detail the features of foam coarsening in two dimensions, before extending the results to three-dimensional foams.

2D foams

Quasi-two-dimensional foams provide the framework for dynamical studies in foam systems. They consist of a single layer of bubbles, which can be experimentally obtained by sandwiching a foam between two rigid plates with a spacing smaller than the bubble size. This way bubbles of a two dimensional dry froth have a polygonal shape, whose sides correspond to films and vertices to vertical Plateau borders. We can distinguish the *internal* Plateau borders, which span vertically the gap between the plates, from the *external* Plateau borders, which spread out horizontally on the plates' surface, as shown in figure 1.6. Euler's theorem relates the number of polygons P, sides S and vertices V by $P - S + V = 2$. This equation, combined with the observation that three sides meet at every vertex and every side connects two vertices, leads to the conclusion that for an infinite 2D foam the average number of sides per polygon is six.

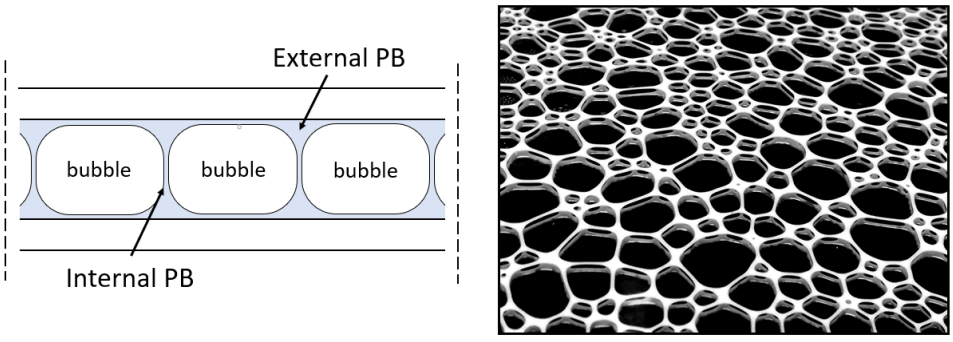

(a) (b)

Figure 1.6: **Quasi-2D foam.** *Picture (a) represents a section of a 2D foam cell, showing the monolayer of bubbles with external and internal Plateau borders. The same structures can be recognised in picture (b), which shows an example of a real 2D coarsening foam, sandwiched between two transparent surfaces.*

What plays a fundamental role in 2D foam coarsening is the topology of the bubble pattern [6] or, more precisely, the number of neighbours of a bubble.
Let us consider a bubble i with n neighbouring bubbles j within a dry 2D foam. We can define the *geometrical charge* of the bubble as the quantity:

$$q = \sum_{j=1}^{n} k_{ij} l_{ij} \tag{1.4}$$

where k_{ij} is the curvature of the edge ij and l_{ij} its length. This quantity is proportional to the *topological charge* $q_t = 6 - n$ that describes the difference from an ordered foam with hexagonal bubbles:

$$q = \sum_{j=1}^{n} k_{ij} l_{ij} = \frac{\pi}{3}(6 - n) = \frac{\pi}{3} q_t \tag{1.5}$$

This relation describes the link between the number of sides of a bubble and its shape. As can be seen in figure 1.7, a bubble with less than six sides has a positive geometric charge, consequently it has convex sides on average. By contrast, bubbles with more than six sides have a negative geometric charge, so their sides are concave. Finally, if all the edges of the bubble are flat, the curvature is equal to zero, then the bubble must be an hexagon.

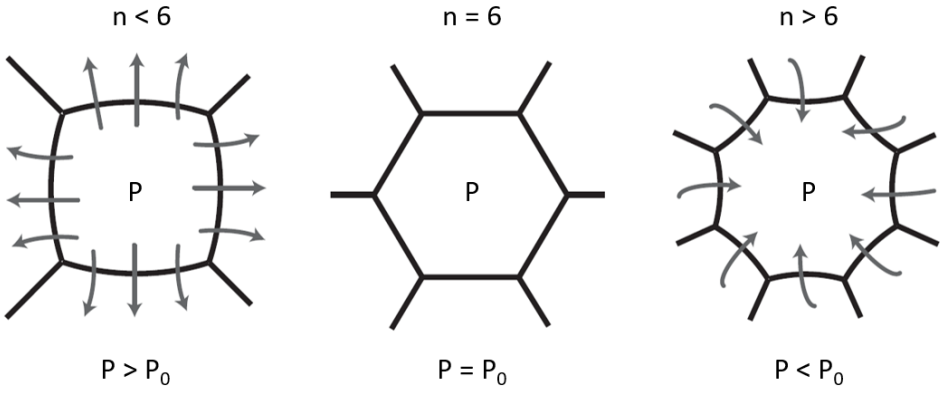

Figure 1.7: **The role of topology.** *Starting from the left, a bubble with less than six neighbours has convex sides, hence Von Neumann results state that its pressure is greater than the average pressure of its neighbours P_0 and it shrinks until it disappears. The curvature of a six-sided bubble is zero on average, therefore its pressure is equal to P_0. Finally, a bubble with more than six sides is concave on average, hence its pressure is lower than its neighbours and it grows.*

A fundamental equation for 2D foams, which links the pressure in a bubble to its shape and to its number of neighbours, was discovered in 1952 by Von Neumann:

$$\sum_{j=1}^{n} \frac{e}{2\lambda}(P_i - P_j)l_{ij} = \sum_{j=1}^{n} k_{ij}l_{ij} = \frac{\pi}{3}(6-n) = q \tag{1.6}$$

where e is the thickness of the 2D foam and λ is the line tension. Bubbles with positive geometric charge consequently have a higher pressure than the average of their neighbours, while bubbles with many sides have a lower pressure than their neighbours.

If the gas diffuses from a bubble i to a neighbouring bubble j only through the film ij, the flux from one bubble to the other will be proportional to $l_{ij}(P_i - P_j)$, that is the product of the driving force (the pressure difference) and the size of the region of gas exchange (the length of the film). If the flux is positive, the amount of gas contained in bubble i decreases, and so does its area A_i, so we can write:

$$\frac{dA_i}{dt} \propto \sum_{j=1}^{n} l_{ij}(P_i - P_j) \tag{1.7}$$

namely the time variation of the area of the bubble i results from the sum of the fluxes to all its n neighbours. By combining this relation with equation (1.6) one can obtain the following remarkable result due to Von Neumann:

$$\frac{dA_i}{dt} = -D_{eff}\, q = \frac{\pi}{3} D_{eff}(n-6) \tag{1.8}$$

which relates topology, geometry, forces and the evolution of the bubble *i*. D_{eff} is the *effective diffusion constant* which is positive and measured in m^2/s. Consequently, bubbles with positive geometric charge lose their gas to bubbles which have more than six sides.

The mentioned effective diffusion constant D_{eff} is proportional to the rate of gas diffusion D_f but it is also related to several other parameters:

$$D_{eff} = D_f \, \frac{2\, He\, \gamma\, V_m}{h}\, a(\epsilon) \tag{1.9}$$

where *He* is the Henry coefficient, which reflects the solubility of the gas in the liquid, V_m is the molar volume of the gas at ambient temperature and pressure, γ is the surface tension, h is the film thickness and $a(\epsilon)$ is a geometric factor which takes into account the liquid fraction [6]. The dimensionless parameter $a(\epsilon)$ expresses the proportion of the bubble surface covered by thin films rather than Plateau borders. It is through this effective surface that gas diffuses from bubble to bubble, since diffusion across Plateau borders is much slower as they are several orders of magnitude thicker. One of the expressions used for $a(\epsilon)$ in the literature [6] is the following:

$$a(\epsilon) = 1 - \left(\frac{\epsilon}{\epsilon^*}\right)^{1/2} \qquad with \qquad \epsilon^* = 0.36 \tag{1.10}$$

3D foams

The results found for 2D foams by Von Neumann can not be generalised in three dimensions exactly as they are. A law that describes the volume variation of a bubble with f facets was found by Mullins [26] [27]:

$$V_f^{-1/3} \frac{dV_f}{dt} = -D_{eff}\, q(f) \tag{1.11}$$

where the D_{eff} is the same effective diffusion coefficient as in 2D and $q(f)$ is the geometric charge of the bubble. Since large bubbles have statistically more faces than small ones, it means that the largest bubbles ($f > 13$) will grow and the smallest bubbles ($f < 13$) will slowly disappear. This leads to a reduction of the number of bubbles and a consequent increase of the average volume of the bubbles left.

This growth process can be described in terms of a statistically self-similar size distribution [26]. Experimental observations [12] show that, after a certain time that depends on the foam, foams that coarsen reach an asymptotic regime in which the average bubble size increases in a simple way. More precisely, for dry foams the mean bubble radius $\langle R \rangle$ evolves like:

$$\langle R(t) \rangle^2 = \langle R(t_0) \rangle^2 + K(t - t_0) \tag{1.12}$$

where the coarsening constant K depends not only on D_{eff} but also on the bubble size distribution. So we can see that for dry foams the average bubble size grows as $t^{1/2}$.

If the foam contains a non negligible amount of liquid, namely if we consider a wet foam, the self similar behaviour is slightly different. The growth process is slowed down by the liquid between bubbles, which acts as a reservoir of gas, resulting in a power law $\langle R \rangle \sim t^{1/3}$. This is called *Ostwald ripening* [6].

Obviously, between these two opposite situations there must be a transition, which is still not well-known, characterised by power laws with intermediate values of time exponent. The lack of theoretical models makes the study of intermediate cases very interesting to probe.

1.4 Controlling and arresting foam ageing

In the previous section we have illustrated the possible mechanisms of foam ageing. Since they destabilise liquid foams and alter their structure, many industrial applications require an in-depth understanding of these processes and of the possible methods to inhibit them. In this section we shall briefly review part of the relevant current background existing in the literature.

A drainage halt has been experimentally observed in foams having a concentrated clay particle suspension as the continuous phase [17]. As found in an interesting paper [5], gravitational foam drainage can be delayed if the yield stress of the continuous phase is higher than the buoyancy force per unit area exerted between the bubble and the liquid

phase, namely $\sim \rho g R/3$. As the foam coarsens, the radii of the bubbles increase and so does the buoyancy force, until the liquid phase starts draining downward.

Coarsening process can be hindered in different ways. Intuitively, a geometrical method consists of generating monodisperse bubbles arranged in almost crystalline structures, where the Laplace pressures in neighbouring bubbles are nearly the same. However, such structures generally present defects which become natural nucleation sites for coarsening.

Alternative methods involve physicochemical features of foams. As we have seen in the previous section, the coarsening rate is fixed by the effective diffusion coefficient D_{eff}. Thus, a way to slow down coarsening consists of reducing the liquid film permeability. For example, permeability results decreased when a dense surfactant monolayer is adsorbed at the liquid/gas interfaces [35]. Alternatively, one can play on the gas phase and use a mixture containing an insoluble gas species: as the soluble gases diffuse out of the bubble, the internal concentration of the insoluble one increases, generating an osmotic pressure that is opposed to the Laplace pressure.

It has been theoretically shown that the dissolution of a bubble can be delayed if the surrounding liquid phase is viscoelastic [16]. Another relevant theoretical study [37] has shown that the kinetics of coarsening is determined by either the rate of gas diffusion or the rate at which bubbles rearrange, with the slowest process determining the bubble growth rate. When the bubble rearrangements are negligible, the gradual increase of elastic stresses among the bubbles can arrest the coarsening of well-separated large bubbles and elastically stabilise the whole foam.

As supposed in [5], coarsening can be in principle arrested if the Laplace pressure is smaller than the yield stress of the continuous phase. However, the halt of coarsening due specifically to the elasticity of the continuous phase has not been experimentally shown.

A recent experimental study [3] has investigated the effect of an elastic continuous phase combined with the use of insoluble gas species. By employing a polymer gel to generate a monodisperse foam, they experimentally observed a slowing down of coarsening. They have found that the stability domain of foam is governed by a critical radius set by the ratio of the surface tension to the foam storage modulus.

The present thesis aims to experimentally probe the impact of an elastic liquid phase on foam coarsening. In the next section we shall better illustrate the conditions we want to work in and how to realise them.

1.5 Avoidance of drainage and coalescence

As we have already stated, the purpose of this study is to understand how the mechanical properties of the liquid phase impact on foam coarsening. Thus, it is necessary to find a way to get rid of drainage and coalescence, which would otherwise affect foam evolution, making difficult to observe and decouple the coarsening.

1.5.1 The storage modulus

Before discussing how to skip undesired mechanisms of foam evolution, let us briefly review some rheological properties of complex fluids.

Let us consider a small volume of fluid, like the one shown in figure 1.8. Imposing a *shear stress* σ on the fluid surface, it will deform and we can define the *shear strain* γ as the tangent of the deformation angle.

If the stress is small enough and the fluid is elastic, it will behave like an elastic solid, namely the strain will be proportional to the applied stress following Hooke's law:

$$\sigma = G\gamma \tag{1.13}$$

and the proportionality factor G is called the *storage modulus*, since it represents the storage of elastic energy inside the fluid. On the other hand, the *strain rate* $\dot{\gamma}$ is linked to the fluid viscosity η by the relation:

$$\sigma = \eta\dot{\gamma} \tag{1.14}$$

meaning that the more viscous the fluid, the slower will be the deformation.

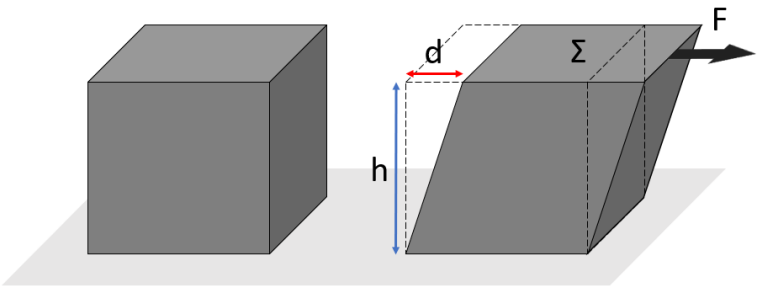

Figure 1.8: **Shear stress and shear strain.** *When a shear stress $\sigma = F/\Sigma$ is applied on the surface of a small portion of fluid, the fluid deformation is represented by the shear strain $\gamma = d/h$. Likewise, if we slightly deform a small element of an elastic fluid, it will answer with a stress proportional to the applied strain.*

In order to avoid drainage during the experiments, the fluid to choose as the continuous medium of our foams must have specific rheological properties. It has to be elastic enough to withstand the hydrostatic pressure inside the Plateau borders $\Delta P_h = \rho g R$ to stop the bubbles from rising and effectively stop drainage. For a typical bubble radius of 400 μm and a liquid density of about 1000 kg/m^3, ΔP_h results approximately 4 Pa. At the same time, if we want the foam to coarsen, the liquid can not be too elastic to contrast the Laplace pressure difference $\Delta P_L = 2\gamma/R$ that, for the same bubble size and a surface tension of around 30 mN/m, assumes an approximate value of 150 Pa. So, if we want drainage to be negligible during coarsening, the storage modulus of the liquid should range between these two values.

Let us now take into account coalescence. Since we know that it is strongly coupled to drainage, we can assume that if the foam does not drain, the liquid fraction remains constant and homogeneous and will not decrease below a critical value during the experiment. Therefore, in the absence of drainage, if the foam is not too dry and an efficient surfactant provides enough stability to the thin films, the foam should not coalesce. The surfactant used in our study is efficient, so we assume that we have negligible coalescence in our system. However, we will monitor the foams during their ageing to ensure that this is true.

1.5.2 Emulsions

In order to provide the right viscoelasticity to the continuous medium, emulsions are chosen to be employed as the liquid phase of foams.

Like foams, emulsions are colloidal dispersions of two immiscible fluids, in which a liquid is dispersed in a continuous liquid phase of different composition [34]. In most emulsions, one of the liquids is aqueous while the other is hydrocarbon and referred to as oil. Two types of emulsion are easily distinguished, depending on which kind of liquid forms the continuous phase: *oil-in-water* (O/W) for oil droplets dispersed in water, *water-in-oil* (W/O) for water droplets dispersed in oil.

Most emulsions are not thermodynamically stable, but quite stable emulsions can be obtained by adding an emulsifying agent or stabiliser, which is usually a surfactant. Surfactants make the emulsion easier to form, but they also provide stability to the droplets by forming a protective film that prevent their breakage and keep their size distribution from changing with time, even when the droplet concentration is changed by dilution. A picture showing a typical O/W emulsion structure is reported in figure 1.9.

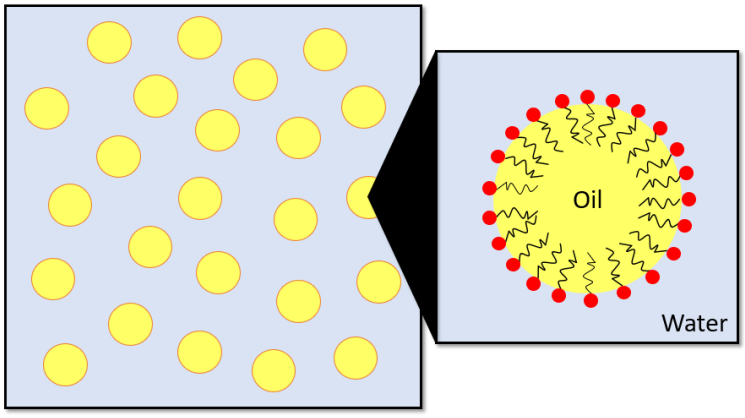

Figure 1.9: **Oil-in-water emulsion.** *The picture sketches the typical structure of a diluted O/W emulsion, with spherical oil droplets dispersed in the aqueous phase. A zoom on a droplet reveals the surfactants adsorbed on the oil/water interface.*

A relevant parameter for O/W emulsions is the *oil volume fraction*, that describes the quantity of oil dispersed in the emulsion. It is defined as the ratio between the volume of oil V_{oil} and the total volume of the emulsion $V_{emulsion}$:

$$\phi = \frac{V_{oil}}{V_{emulsion}} \tag{1.15}$$

This parameter can span values from zero to almost one. At low oil fractions, emulsions consist of unpacked spherical droplets, like the ones shown in figure 1.9, but owing to the deformability of the droplets, they may be concentrated up to oil fractions much higher than the volume fraction of randomly close packed hard spheres $\phi^* = 0.64$.

When ϕ exceeds ϕ^*, the oil droplets deform and as ϕ tends to one the continuous phase of the emulsion is confined to thin films between deformed droplets, resembling the liquid films of a foam.

Increasing systematically the volume fraction of droplets, one expects eventually to find a point of phase inversion where the oil becomes the continuous phase. This can be avoided by the surfactant adsorbed onto the droplets interfaces, which allows the emulsion to remain stable even when the oil fraction approaches unity [22].

Despite being composed solely of fluids, at high droplet concentrations emulsions can possess a shear rigidity and act like an elastic solid [4]. This elasticity exists only when the repulsive droplets have been concentrated to a volume fraction ϕ sufficiently large to permit the storage of interfacial energy from an additional deformation of the shape induced by an applied strain. The energy scale that controls this deformation is the Laplace pressure of the droplets γ/R, where γ is the surface tension and R is the radius of the undeformed droplets.

The key to the origin of the elastic modulus of an emulsion is its dependence on ϕ. The analogy between emulsion and foam structure suggests that, for ϕ approaching to one, an emulsion should act like a dry foam, where the elasticity results entirely from the stretching of the interfaces. In the literature [24], it has been found experimentally that the storage modulus of a monodisperse emulsion shows a universal dependence on ϕ when scaled by the Laplace pressure, following the relation:

$$G' \sim \phi(\phi - \phi^*)\frac{\gamma}{R} \tag{1.16}$$

This scaling confirms that the elasticity of compressed monodisperse emulsions arises from the storage of energy at the droplets interfaces and that it depends only on the packing geometry of the droplets.

These rheological properties of emulsions at high oil fractions, make them the best candidate for the continuous phase of our foams. Their storage modulus is in fact in the right range for our purposes, as will be experimentally verified in §3.1. We shall study foamed emulsions at different oil fractions, to investigate the impact of emulsion elasticity on foam coarsening.

2 Experimental approach

In this chapter, we shall describe all the materials and experimental techniques used for the present study. We shall start from emulsion characterisation, by describing their composition, their generation process and their rheological investigation. We shall then switch to foams, describing first their creation and then the methods used to measure the bubble size evolution. For this purpose, we carried out both imaging and spectroscopy experiments, hence a short description of the main features of diffusing-wave spectroscopy is given. Then we shall explain the realisation of 2D foams and the set-up used for studying such systems. A description of the image treatment is provided in each case.

2.1 Emulsions

The emulsions used as the liquid phase of foams are O/W emulsions at high oil fractions. The oil used to prepare them is commercial rapeseed oil (Leader Price distribution). We chose to employ a commercial oil because of the large quantity of emulsion needed to produce foam with our method and, since we are interested in bulk properties, potential impurities should not affect substantially our results. Rapeseed oil has a density of 0.91 g/cm^3 and a surface tension of 33.8 mN/m at 20^{o}C, as reported in the literature [13].

The surfactant used in the present thesis is Sodium Dodecyl Sulphate (SDS, Sigma-Aldrich), also known as Sodium Lauryl Sulphate, that is how it appears on the labels of most commercial cleaning products. This is an anionic surfactant, meaning that it carries a negative electrostatic charge, and it is formed by a 12-carbon tail attached to a sulphate group, as shown in figure 2.1. Some physical and chemical characteristics of rapeseed oil and SDS are summarised in table 2.1.

The aqueous surfactant solution was prepared by dissolving SDS in ultra-pure water at a concentration 20 g/L, which corresponds to approximately ten times its critical micelle concentration. The millipore water, with a 18.2 MΩ resistivity, was freshly obtained from a specific filtering device (Purelab Flex).

Rapeseed oil		
T [^{o}C]	ρ [g/cm^3]	γ [mN/m]
20	0.9145	33.8
30	0.9080	33.0
40	0.9027	32.1

(a)

Sodium Dodecyl Sulfate	
Density	1.01 g/cm^3
Molar mass	288.38 g/mol
cmc @ 25^{o}C	8.2 mM
Solubility	200 mg/ml

(b)

Table 2.1: **Physical and chemical features.** *Density and surface tension at different temperatures for rapeseed oil from [13] (a). Some parameters for SDS (b); solubility and cmc are meant in pure water.*

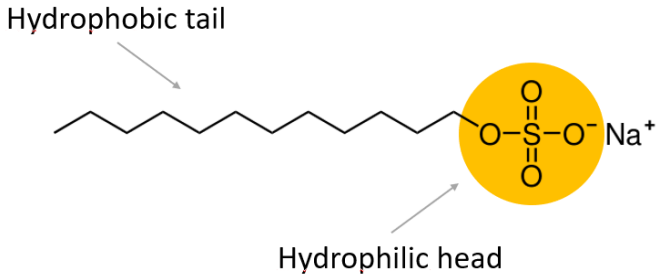

Figure 2.1: **Sodium Dodecyl Sulfate.** *The picture shows the molecular structure of the anionic surfactant, with the hydrophobic carbon-tail and the hydrophilic polar head. Its chemical formula is* $CH_3(CH_2)_{11}SO_4\ Na$.

2.1.1 Generation

There are several ways for preparing emulsions in the literature. Basically, one can mechanically blend the different components or induce phase separation by thermal quench or by chemical reactions [22]. In our case emulsions were prepared by mechanically mixing the two different liquids by using the so-called two syringes method.

The technique consists of two syringes (60 ml, Codan Medical) connected by a short piece of tube, as shown in figure 2.2, which are filled with well-defined volumes of rapeseed oil and SDS solution, corresponding to the desired oil fraction. The emulsification occurs by pushing both liquids repeatedly through the connection at least ten times. The outlets of the syringes are thinner than the connecting tube, so they form constrictions in the flow path leading to emulsion generation. For spectroscopy experiments, this pushing action was automated by using a custom-made machine [15], while for all other experiments this procedure was made by hand. The emulsions obtained with this technique result polydisperse.

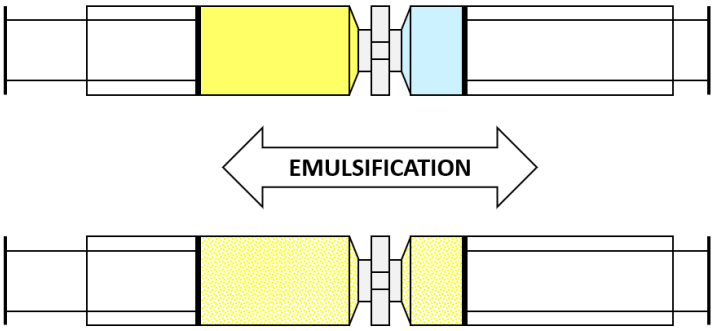

Figure 2.2: **The two syringes method.** *Syringes are first filled with the desired quantities of oil and surfactant solution, then connected by a short junction. Emulsification occurs by pushing repeatedly both liquids through the connection.*

2.1.2 Rheology

As commonly done in the literature, the rheological properties of the emulsions were probed by performing rheological strain sweep tests [25], which allow to get the G' and the G'' moduli by imposing an oscillatory shear in a cylindrical Couette geometry, like the one shown in figure 2.3, and measuring the resulting stress.

A sinusoidal strain of increasing amplitude $\gamma(t)$ is applied by rotating the inner cylinder at constant frequency ω equal to 1 rad/s, while the external cup is kept stationary.

If the strain amplitude is sufficiently small that the fluid is not much disturbed by the deformation, then the resulting stress $\sigma(t)$ measured during the oscillations is controlled by the rates of spontaneous rearrangements inside the fluid. Hence the shear stress will be sinusoidal as well, with an amplitude proportional to the amplitude of the applied strain:

$$\sigma(t) = \gamma(t)[G'(\omega)sin(\omega t) + G''(\omega)cos(\omega t)] \tag{2.1}$$

The first term is in phase with the strain γ and is proportional to the storage modulus G', whereas the second term is in phase with the strain rate $\dot{\gamma}$ and is proportional to the loss modulus G'' that represents the viscous dissipation.

All the measurements were performed with a compact rheometer (Physica MCR 301 by Anton Paar). To avoid emulsion slippage when imposing the strain, the surface of the inner cylinder has been sand blasted to make it rough. The temperature, controlled by a Peltier device, was fixed to $(21.0 \pm 0.5)^o$C for each probe.

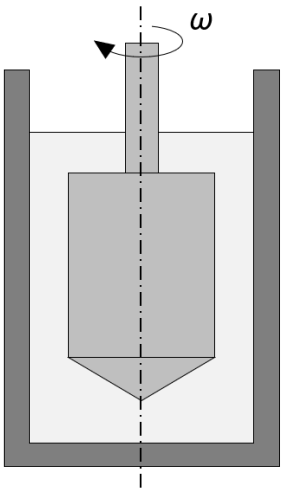

Figure 2.3: **Couette geometry.** *The picture shows a section of the cylindrical Couette geometry employed for the strain sweep tests. The inner cylinder rotates with constant frequency ω and time-increasing amplitude. Its rough surface drags the emulsion inside the gap and the resulting stress is measured, in order to get the G' and G'' moduli.*

2.2 Foam generation

There are several methods to generate foams in the literature [10], but the use of a planetary mixer represents the most efficient way for foaming viscous and viscoelastic fluids [29].
After emulsion preparation, foams were then created by using a kitchen mixer (Kenwood Multione). This familiar device is equipped with a whisk that rotates simultaneously around two different axes: as shown at the top of figure 2.4, the primary axis of rotation is the axis of the mixing tool, while the second one is located at the centre of the vessel containing the foaming emulsion.

The foaming process is displayed at the bottom of figure 2.4. Basically, the mechanism of air entrapment can be described as follows. The double rotation of the mixing tool generates waves on the surface of the foamed emulsion. These surface waves produce cavities which are then covered by other foam layers dragged by the metal rods of the mixing tool, leading to the formation of large air pockets. These air pockets are then gradually broken down into smaller bubbles under the action of the shear forces inside the agitated foam. The two processes of air entrapment and bubble breakage occur simultaneously, ensuring an increase of the air volume fraction inside the foam and a gradual decrease of the mean bubble size [29]. Foams are always created by gradually increasing the rotation speed from the lowest to the highest level, then leaving the mixer running at maximum speed for at least half an hour. The final result is a large amount of foam which is quite dry but very polydisperse.

Unfortunately, this foaming method does not allow to set a specific liquid fraction a priori, but we can evaluate it once the foam is created. Thus, in order to quantify the final foam dryness, the volume liquid fraction is measured by weighing a known volume of foam, using a scientific scale with an accuracy of 0.01 g. Knowing the density of the rapeseed oil and taking into account the different oil fractions for each emulsion, we can easily estimate the volume of the emulsion contained in the foam sample. Dividing by the total volume, we finally get the liquid fraction. The use of the mixer allows to get quite dry foamed emulsions, with liquid fractions down to 8%.

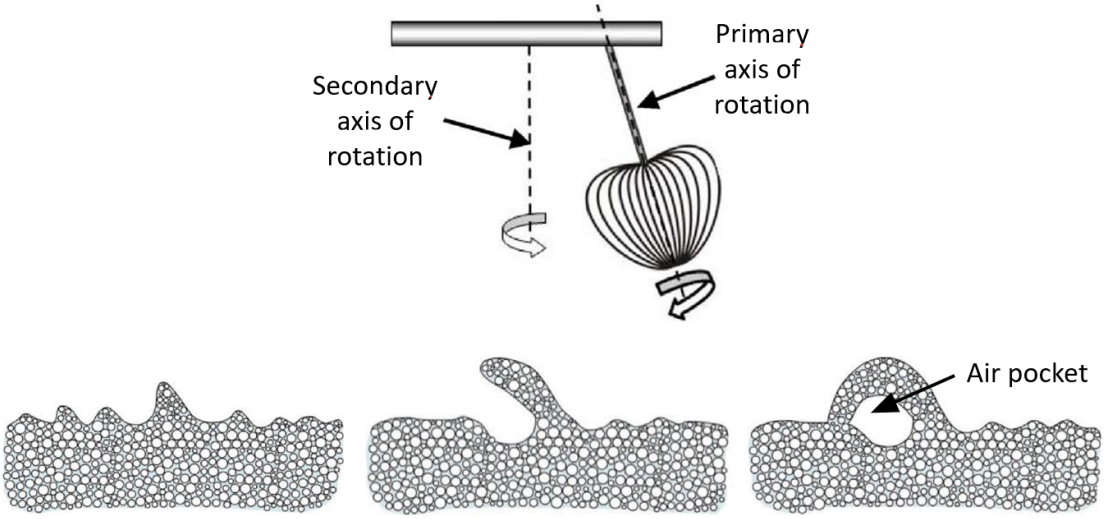

Figure 2.4: **Foam generation process.** *The top figure shows the double axis of rotation of the mixing whisk. At the bottom, a sequence of pictures displays how the waves on the emulsion surface generate air pockets, leading to foam creation.*

2.3 Measuring the bubble size

Transparent foams do not exist. The gas/liquid interfaces inside a foam sample cause light to reflect and refract many times during the crossing. A direct visualisation of the internal structure of a three dimensional foam is then precluded by this unavoidable multiple scattering of light, which gives bulk foams their familiar white opaque appearance.

However, if we want to study foam coarsening, we need to follow the time evolution of the average bubble size inside the sample. For studying highly scattering media like foams, alternative optical methods have been developed and systematically studied, like diffuse-transmission [20] and diffusing-wave spectroscopy [28].

In the following subsection we shall briefly illustrate the basic principles which lie behind diffusing-wave spectroscopy, the main tool we used for studying 3D foams in the present thesis, showing how it provides a non-invasive probe of the structure and dynamics of the foam which allows to follow its time evolution.

In order to check whether there was coalescence or not in the foam samples, for each experiment we simultaneously took pictures of another sample of the same foam. In §2.3.2 we shall explain how we could also get information on the average bubble size evolution from those pictures, which constitute a further check for spectroscopy results.

2.3.1 Diffusing Wave Spectroscopy

Diffusing-wave spectroscopy (DWS) is a photon-correlation technique, that exploits multiple light scattering to probe the internal structure and rearrangements inside very turbid media [38] and it has been widely used for studying foam systems. It is based on the strong assumption that the propagation of light in such media can be described as a diffusion process: each photon is scattered many times before exiting the sample and executes a many-step random walk as it travels through it.

In this approximation, the light transport is described by a diffusion equation, with a diffusivity given by $D = c\,l^*/3$, where c is the speed of light in the medium and l^* is the photon transport mean free path, that can be thought of as the average distance a photon can travel before its direction and phase are completely randomised. This way, all the effects of interference of the fields within the medium are neglected.

An experimental study [36] has shown how the key parameters of photon transport depend on the foam strucure and composition. They found a direct proportionality between the mean free path l^* and the mean bubble radius R, with a constant that depends on the liquid fraction ϵ:

$$\frac{l^*}{2R} = \sqrt{\frac{1}{\epsilon}} \tag{2.2}$$

This means that light is scattered more strongly by wetter foams. Deviations from this rule occur for very dry or very wet foams, since this result holds under the assumption that the film thickness is small compared to the radius of curvature of the Plateau borders and that the latter is small compared to the radius of the bubbles.

Let us consider a foam sample of thickness e crossed by a coherent light beam. If $e >> l^*$, the transmitted light intensity will be approximately proportional to the ratio l^*/e and so proportional to the bubble radius R. Therefore one can write the relation:

$$I(t) \propto \langle R(t) \rangle \tag{2.3}$$

which shows how it is possible to learn information about the foam structure evolution by simply detecting the transmitted light intensity and it has been experimentally verified for quite dry foams [12].

The diffusive propagation of light helps not only in the analysis of the time average of the transmitted light intensity. DWS is a powerful tool also for the investigation of structural rearrangements inside the foam. As the foam coarsens and packing conditions change, local stress differences grow until a structural rearrangement occurs. This technique allows to get information about the internal dynamics by interpreting the temporal fluctuations of light through the photon autocorrelation function [11].

However, the physical system under investigation does not contain only two phases like a traditional aqueous foam: the choice of employing an emulsion as the continuous medium makes the treatment of the correlation function more complicated, as one needs to decouple the rearrangements of bubbles from the local rearrangements of the oil droplets dispersed in the Plateau borders. In the present thesis we focus only on the bulk structure evolution of foamed emulsions, namely we look at how the mean bubble radius changes over time by exploiting only diffusive light transmission.

Experimental set-up

All the diffusing-wave spectroscopy experiments were carried out in a transmission configuration set-up, that is sketched in figure 2.5. Coherent green light of wavelength $\lambda = 515$ nm, provided by a IIIb class laser (Compass 315M-100), crosses a series of filters (ThorLabs) to reduce stray rays and adjust incident light intensity, before being reflected 90^o by a mirror placed at 45^o respect to the optical path. The light beam is then spread by a divergent lens onto the foam sample and undergoes multiple scattering mainly due to the liquid/gas interfaces inside the foam. The transmitted light is detected and amplified by a photomultiplier (PMT-120-OP/B) which is linked to a digital correlator (Flex03lq-12), in order to obtain the intensity over time and the photon autocorrelation function. During the experiments everything was covered by a black curtain. The foam cells used for DWS experiments were obtained from a square Petri dish by gluing a joint of gum of thickness $e = 20\ mm$. This sample thickness is not always much larger than the mean bubble radius R of our foamed emulsions, but thanks to the presence of the oil droplets dispersed in the liquid phase, which in turn scatter light, the diffusion limit is ensured.

2.3.2 Imaging

After foam generation, we filled not only the cell for DWS, but also a second sample of thickness 10 mm for monitoring foams via imaging. The foam cell is illuminated by transmission of white light by a LED lamp placed under the cell. Sequences of pictures, with a 2560x1920 pixels resolution, were taken at constant frame rate by a camera (uEye, model UI-148xSE-C) orthogonal to the sample surface and equipped with a suitable objective (Ricoh, Lens Pentax C2514-5M, 1.4/25mm). This way we could make a video of the foam ageing to check if coalescence was negligible.

By analysing these pictures, we could also learn information about the average bubble size inside the sample. Of course, this method takes into account only the boundary bubbles which are in contact with the cell surface. Pictures of the DWS samples were also taken at the end of each experiment to calibrate the curves obtained by spectroscopy.

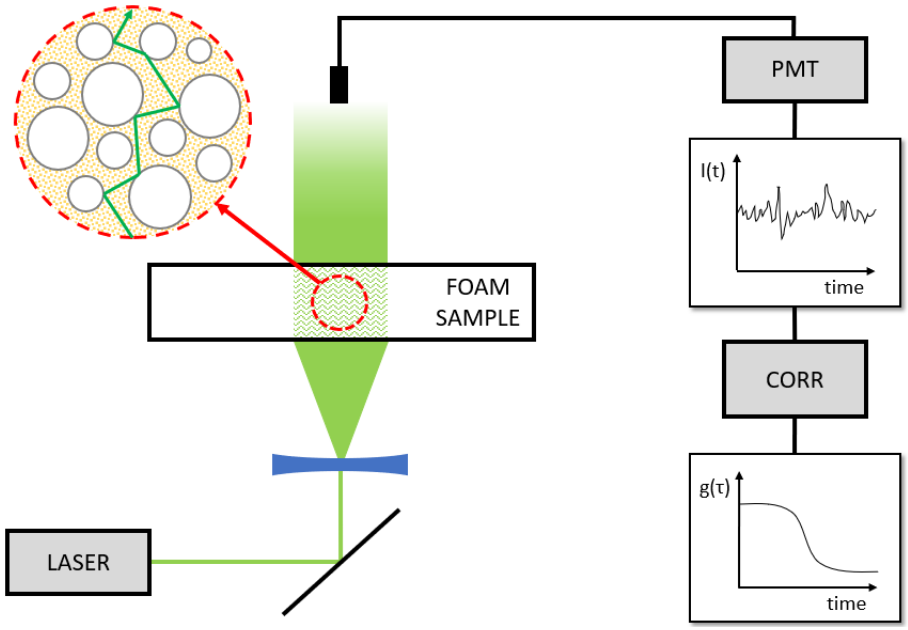

Figure 2.5: **DWS set-up.** *The picture shows a diagram of the experimental set-up used for diffusing-wave spectroscopy. A coherent green light beam crosses the foam sample and the transmitted light intensity is detected and properly amplified by a photomultiplier. A digital correlator records also the photon autocorrelation function.*

Image treatment

Image treatment is divided in two steps. First, pictures are pre-treated by adjusting the brightness and enhancing the contrast with ImageJ, in order to better identify the borders of the surfacial bubbles. Then, a custom-made Matlab program, basically based on the available function *imfindcircles*, is used to recognise the bubbles by finding the circles on the pictures, after setting reasonable ranges of radii. An example of the basic steps of image treatment for one picture are shown in figure 2.6: one can see the original picture (a) and the same one after contrast and brightness adjustment (b), while the overlap of the circles detected by the Matlab program is shown in (c).

Since the foam sample is three dimensional, the program detects some circles also from the underlying layers of bubbles; moreover, the contact with the surface results in a deformation of boundary bubbles shape, so that the program is unable to detect some very big bubbles that are not perfectly round.

For these reasons, this method is not accurate enough for directly studying the foam evolution, as already stated at the beginning of this section, hence we used it only as a further check. Anyway, we used this method also to obtain an average bubble radius for calibrating DWS results: another way to do this would have been observing under a microscope a small sample of freshly created foam. However, if the foam is quite dry, bubbles are tightly packed together so that if we want bubbles to appear as circles, that could be analysed even directly with ImageJ, the foam on the glass slide needs to be

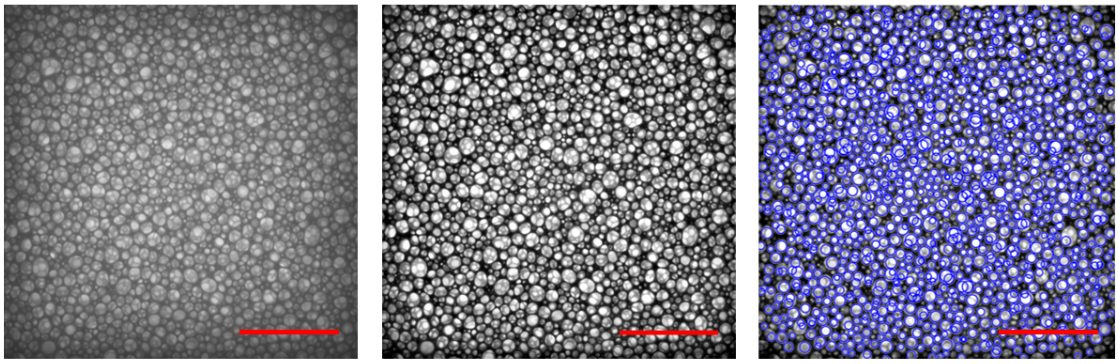

(a) (b) (c)

Figure 2.6: **Image treatment.** *An example of image treatment for a 3D foamed emulsion having $\phi = 80\%$ and $\epsilon = 9\%$. The brightness and the contrast of the original cropped picture (a) are adjusted in order to enhance the sharpness of the surfacial bubble borders (b). Then the Matlab program detects the bubbles on the sample surface by finding circles in the picture (c). Scale bars 20 mm.*

strongly diluted, obtaining pictures with only less than ten bubbles per image. Hence, to have a good statistics it is easy to understand that we would need to prepare hundreds of slides, so this method would be more accurate but not efficient. Using the rough 3D imaging method, instead, it is possible to get more than a thousand of bubble radii from only one picture, providing a good statistics even if the method is not so accurate.

Error on the mean bubble radius

In order to roughly estimate the maximum error committed with this Matlab treatment, we can take a picture for which the Matlab program seems to not recognise very well the surfacial bubbles and try to perform a different analysis.

For example, let us consider a foamed emulsion having 70% of oil fraction. As shown in figure 2.7, by using ImageJ we crop a central square portion of the original picture and we literally count the number of surfacial bubbles, without taking into account the bubbles appearing from the inner layers. Then we adjust the contrast and we binarise the picture. This way, from the number of white pixels and knowing the total number of bubbles, we can estimate an average bubble radius using the following relations:

$$A_w = N \cdot \pi R^2 \quad , \qquad R = \sqrt{\frac{A_w}{N \cdot \pi}} \tag{2.4}$$

where A_w is the total number of white pixels of the picture and N is the total number of bubbles counted on the surface. For the picture considered in figure 2.7, A_w is found to be 255756 pixels, N is 421 and R results equal to 14 pixels, corresponding to a radius of 0.61 mm. The radius found with the Matlab program is equal to 0.86 mm. The difference between the two values is 0.25 mm, which is approximately the 30% of the Matlab mean radius.

This manual procedure provides less statistics and leads to the unavoidable problem of the boundary bubbles: wherever you crop the picture, there will always be portions of cropped bubbles on the boundaries which contribute to the white pixel fraction. If one does not count the boundary bubbles, the final mean radius is over estimated, while if one does count them the radius value will be under estimated.

We highlight that measuring the bubble size in turbid media is usually complicated and since in our case foam dilution is not efficient, there are no other excellent techniques to get an average bubble radius. Therefore we shall use the Matlab program to get a rough estimation of the average bubble size from the pictures and we shall assume a margin of error equal to 30% for the so-calculated absolute values of the mean bubble radii.

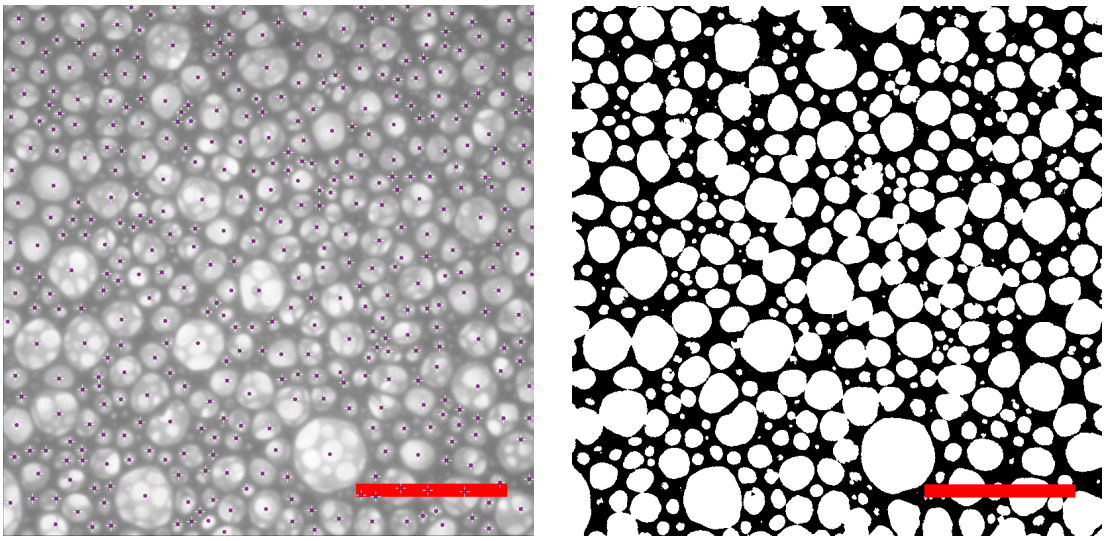

(a) (b)

Figure 2.7: **Mean radius error bar.** *Figure (a) shows a portion of 800x800 pixels of the original picture of a 3D foamed emulsion of ϕ =70%. A manual counting of surfacial bubbles gives a total number N equal to 421. Figure (b) shows the same portion but binarised after contrast enhancing. From the latter it is possible to count the number of white pixels, which roughly corresponds to the total area of bubbles, and to find an average of the bubble radii. The mean radius is found to be 0.61 mm which is much smaller than the value 0.86 mm obtained with Matlab. Scale bars 10 mm.*

2.4 2D foam set-up

To study the film permeability we need to focus on a quasi-2D foam system. Basically, we need to follow the time evolution of the 2D bubble area, which depends on the number of the neighbours, as stated by Von Neumann's relations. To do that, it is necessary to take sequences of pictures at constant time intervals, namely to carry out an imaging experiment with a very simple set-up, which is shown in figure 2.8.

Among all the possible configurations for a 2D foam [6], we chose to use a *Hele-Shaw* cell, that consists of two solid flat plates filled with a monolayer of bubbles. The cell used, that is shown in figure 2.8 (a), has a glass surface on the bottom and a polycarbonate one on the top and is equipped with a reservoir that can be filled with the liquid phase to keep the capillary pressure constant. By injecting gas at a constant rate from the bottom of the liquid chamber, it is possible to obtain a monodisperse 2D foam, with a bubble size depending on the needle diameter. The boundary of the cell is made of a gum junction with a constant thickness.

As shown by the diagram in figure 2.8 (b), the sample is homogeneously illuminated from above by a square distribution of LEDs. The camera (uEye, model UI-225xSE-C), equipped with a suitable objective (Fujinon, model HF16SA-1, 1.4/16mm), is arranged above, orthogonally to the foam cell and allows to get pictures with a 1600x1200 pixels resolution. During the experiment everything is covered by a black curtain to avoid undesired light reflections. For studying 2D foamed emulsions we first generated the foam using the mixer and then we carefully filled the cell without using the reservoir. This way the foam was polydisperse and its liquid fraction was kept constant during the experiment.

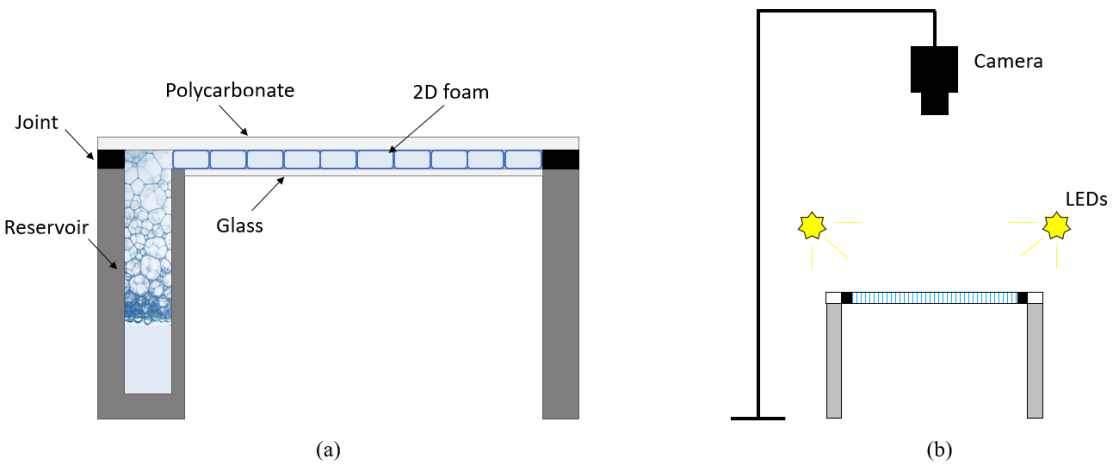

Figure 2.8: **2D foam set-up.** *On the left one can see a section of the Hele-Shaw cell used for the 2D foam experiments (a). Air bubbles are injected through a needle on the bottom of the reservoir. The picture on the right shows a section of the whole set-up (b). A camera takes photographs of the 2D foam inside the cell, which is illuminated from above through a distribution of LEDs.*

Image treatment

Images are first treated using ImageJ. An example of the fundamental steps is reported in figure 2.9. After enhancing the contrast, the grey pictures are binarised, namely made only of black and white pixels. Then, the threshold is properly adjusted to get all the bubbles well delimited and closed. After that, the pictures are inverted and, thanks to the ImageJ function *skeletonize*, the skeleton of the 2D foam is obtained. The bubbles in these images are separated from each other by closed black lines of pixels over a white background. In order to follow the temporal evolution, skeletonized images of 2D foams are then analysed by using a custom-made Matlab program, developed by Emilie Forel in her PhD thesis [14]. This program recognises and follows the bubbles along the images sequence. It also finds the nodes and the number of neighbours for each bubble. A sequence of further Matlab programs is then used to elaborate the results.

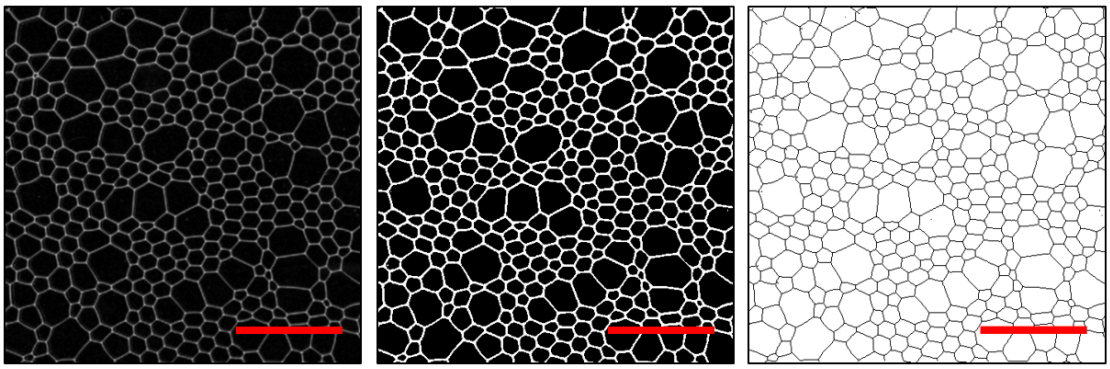

Figure 2.9: **Image pre-treatment.** *An example of image treatment for a 2D foam made of Fairy solution. The original picture is first cropped and the background is subtracted (a). Then image contrast is enhanced and the picture is binarised, adjusting the threshold to get all the bubbles well closed (b). Finally, the picture is inverted and skeletonized (c). Scale bars 20 mm.*

3 Results

In this chapter we shall present all the experimental results obtained from our investigation. We shall start from emulsion behaviour under sweep tests. We will then present how our foamed emulsions age, showing the time evolution of the bubble radius obtained from diffusing-wave spectroscopy. Then we shall switch to the results of the film permeability obtained from 2D foam experiments. In both cases we will first compare the results obtained for well-known standard systems with their corresponding behaviour in literature.

3.1 Emulsion viscoelasticity

As explained in §2.1.2, we first performed rheological sweep tests to investigate emulsion viscoelasticity. Figure 3.1 displays the results obtained for emulsions having different oil fractions. For each emulsion, both the storage modulus G' and the loss modulus G'' are reported in the graph for shear strains with increasing amplitude.

For low strain values, we are in the so-called linear regime, where the modulus G' is constant. Here, the graph shows a G' greater than G'', reflecting the elastic nature of the emulsion. At larger strains, there is a gradual drop in the storage modulus, while the loss modulus begins to rise. This indicates that the emulsion starts yielding and the flow becomes plastic, as the droplet deformation can no longer take the strain and store elastic energy. At very large strains, beyond the yield point marked by the drop in G', the dominance of G'' reflects the prevalence of the viscous behaviour, which causes energy loss during the flow.

It is easy to see how the storage modulus G' increases with the oil fraction, meaning that as the concentration of oil droplets rises the emulsion becomes more elastic, as expected. In order to make visually clear its dependence on ϕ, in figure 3.2 we plot the G' values calculated in the linear regime for different emulsion oil fractions. The G' values are also tabulated in table 3.1.

Let us consider the yield point. The most proper way to measure the yield stress σ_y would be performing experiments with continuous shear. However, it is possible to get an estimation of σ_y also from oscillatory strain tests and it is quite common in the literature [19]. One first has to calculate the yield strain and then multiply by the elastic modulus in the linear regime.

A conventional way to quickly estimate the yield strain is to consider the point where G'' becomes higher than G', namely where the two curves meet, that is properly named *flow point*. Neverthless, it is more usual to consider only the curve of the storage modulus G' in the double logarithmic scale and draw two straight lines in the graph and take the intersection as the yield point. By following the latter procedure, we get the values for the yield strain γ_y and the yield stress σ_y reported in table 3.1.

Furthermore, from figure 3.1 and table 3.1 we can see that if we take into account oil fractions above 70%, the respective storage moduli span values between 10 Pa and 100 Pa, that perfectly fall in the suitable range where we should observe foam coarsening without drainage, as discussed in §1.5.1. Hence we shall focus on emulsions at ϕ higher than 70%.

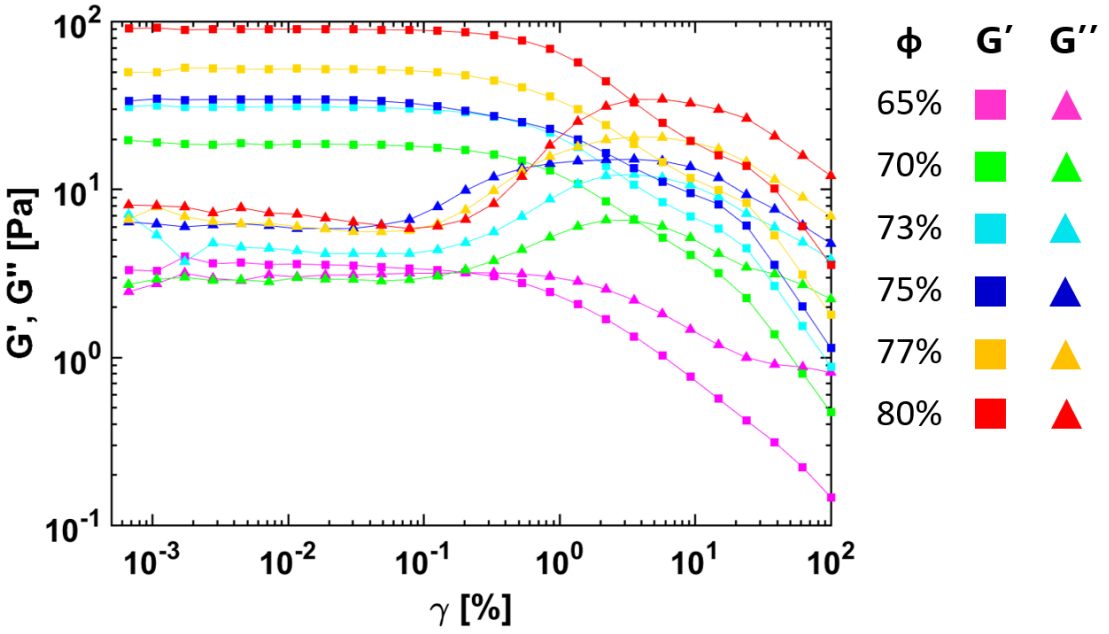

Figure 3.1: **Emulsions rheology.** *The picture shows the results of the rheological sweep tests. The graph compares the emulsion response to increasing strains γ at different oil fractions ϕ, by showing both the storage and loss moduli recorded for each sample. For low strains, one can see that the storage modulus G' increases with the oil fraction, meaning that the emulsion becomes more elastic. For higher strains, beyond the emulsion yield point marked by the drop of the storage modulus G', the rise of the loss modulus G'' represents the dominance of viscous behaviour and the emulsion flow becomes plastic.*

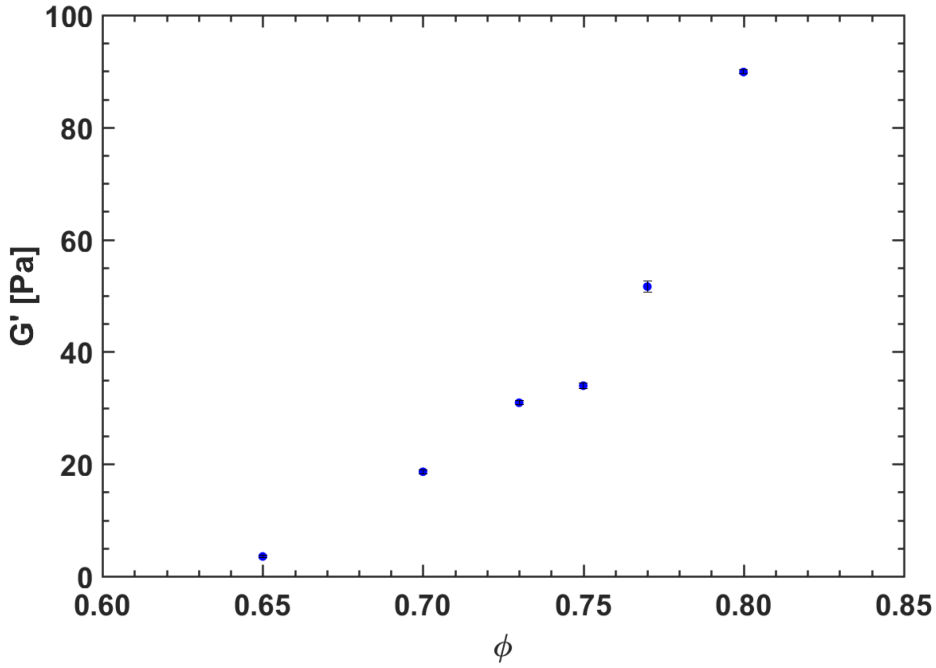

Figure 3.2: G' **dependence on** ϕ**.** *The plot shows the values of the emulsion storage modulus* G' *in the linear regime at different oil fractions* ϕ*. One can see clearly that* G' *increases with the increase of the oil droplet concentration.*

ϕ [%]	G' [Pa]	γ_y [%]	σ_y [Pa]
65	3.5 ± 0.2	0.8	0.04
70	18.6 ± 0.4	0.5	0.09
73	30.9 ± 0.3	0.6	0.19
75	34.0 ± 0.5	0.4	0.14
77	51.6 ± 0.9	0.5	0.26
80	89.9 ± 0.7	0.6	0.54

Table 3.1: **Emulsion rheology.** *The table reports the values found for the storage modulus* G' *from rheological tests at different emulsion oil fractions* ϕ*. It also reports the approximate values for the yield strain* γ_y *and the yield stress* σ_y*, found with the conventional graphical method illustrated in the text.*

3.2 Bubble size evolution

Before presenting the outcome of our investigation about 3D foamed emulsions, we report the results of a well-known standard foam.

Gillette foam

First of all, we studied coarsening in a commercial brand shaving foam, Gillette Series, which easily provides reproducible and cheap foam samples. This commercial foam has been already employed in experimental studies in the literature [12], mainly because of its high stability due to its chemical composition. Its key ingredients (water, stearic acid, SDS, triethanolamine and hydrocarbon gases) produce a foam with approximately 92% of gas fraction [12]. The gravitational drainage in Gillette foam is very slow and we can even ignore it completely on the time-scale of the experiments.

We carried out a DWS experiment for a foam sample of thickness 10 mm. The sample thickness e was chosen in order to satisfy the diffusion condition $e >> l^*$, where l^* is the photon mean free path already defined in §2.3.1. Knowing that l^* is proportional to the mean bubble diameter [36], that for a freshly made Gillette foam is of the order of 40 μm [12], we can see that the diffusion assumption is ensured.

The DWS set-up allows to get the transmitted light intensity over time. The software allows to sample the intensity over time intervals Δt of custom length. An example of the detected intensity for one interval is reported in figure 3.3, where the intensity is averaged over a time interval of 300 s.

By averaging the intensity over those intervals, one can rebuild the trend of the mean intensity over time. Since we expect coarsening to have a higher rate before starting to show the scaling behaviour, the time interval can be changed during the experiment. We set a shorter Δt at the beginning and a longer one at the end, so that the intensity can be considered approximately constant in each time sample. The standard deviation is assumed as the error of the averaged intensity, and it oscillates between the 4% and 10% of the mean value, mainly depending on the length of the time intervals but also on the filters used for partially shielding the laser light impinging on the sample, in order to prevent photomultiplier damage.

As seen in §2.3.1, we know that there exist a proportional relation between the mean bubble radius and the transmitted intensity. Since we are interested in the scaling behaviour, we can normalise the mean intensity values I_t, dividing them by the average intensity I_0 corresponding to the first time interval of the experiment. This way the trend of I_t/I_0 will give the trend of $\langle R_t \rangle / \langle R_0 \rangle$, where $\langle R_0 \rangle$ is the mean bubble radius of the foam sample at the beginning of the experiment.

Results for the Gillette foam sample are shown in figure 3.4. The temporal axis indicates the time after foam creation. The intensities were averaged over time intervals of 300 s at the beginning, 600 s in the middle and 1200 s at the end. One can see that Gillette foam shows an asymptotic behaviour well-described by a power law. Thus, we analysed the trend by fitting the data within the self-similar regime with a curve $y = a \cdot t^b + c$. The fit parameters are reported in table 3.2. We found an exponent b

equal to 0.43 ± 0.05, which falls slightly below the theoretical prediction 1/2 for a dry foam. This happens because Gillette foam is not perfectly dry, having a liquid fraction of 8%. Thus, the power law shown by the mean radius growth should reasonably lie between the 1/2 exponent predicted for a dry foam and 1/3 expected for a wet one. We highlight that our result is perfectly according to the experimental exponent z=0.45 ± 0.05 found in the literature [12].

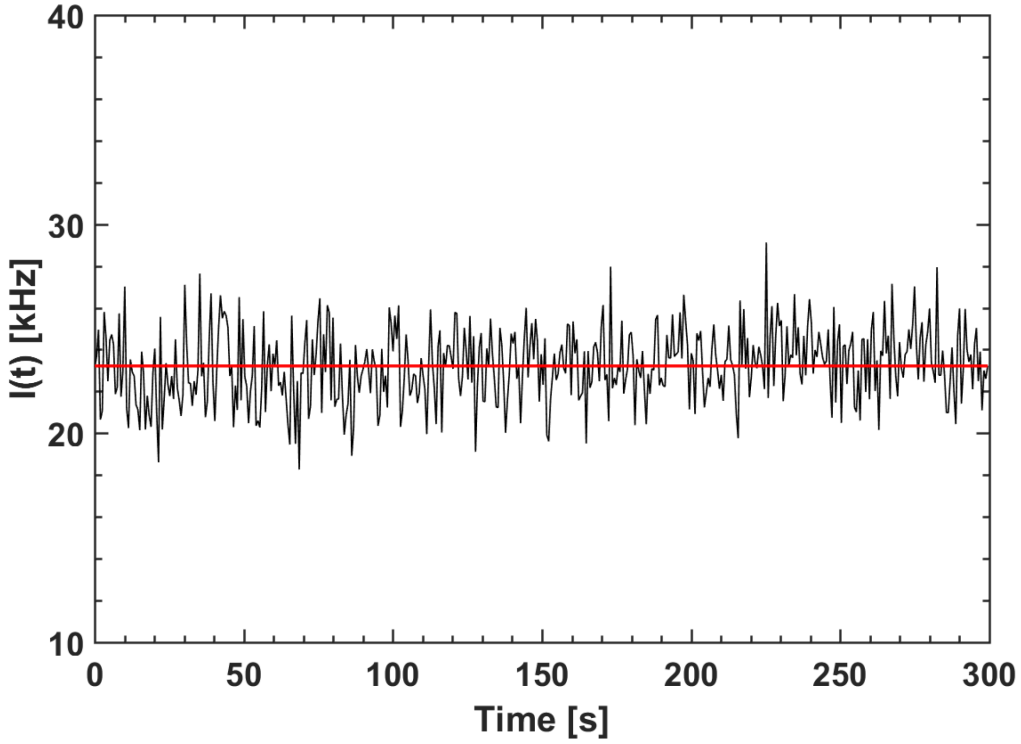

Figure 3.3: **Intensity over a time interval.** *The plot shows the transmitted light intensity detected during the first time interval (300 s) of the DWS experiment carried out for Gillette foam. The red line represents the average, which is equal to (23 ± 2) kHz, where the error corresponds to the standard deviation and results about the 8% of the mean value.*

Before concluding this section, we highlight that we have reproduced results for Gillette foam from literature. Now that we have validated our DWS set-up, we can start investigating the system of interest, namely foamed emulsions. This system presents a peculiarity which makes it different from a standard foam, since foamed emulsions are characterised by the presence of two diffusing species: oil droplets and air bubbles.

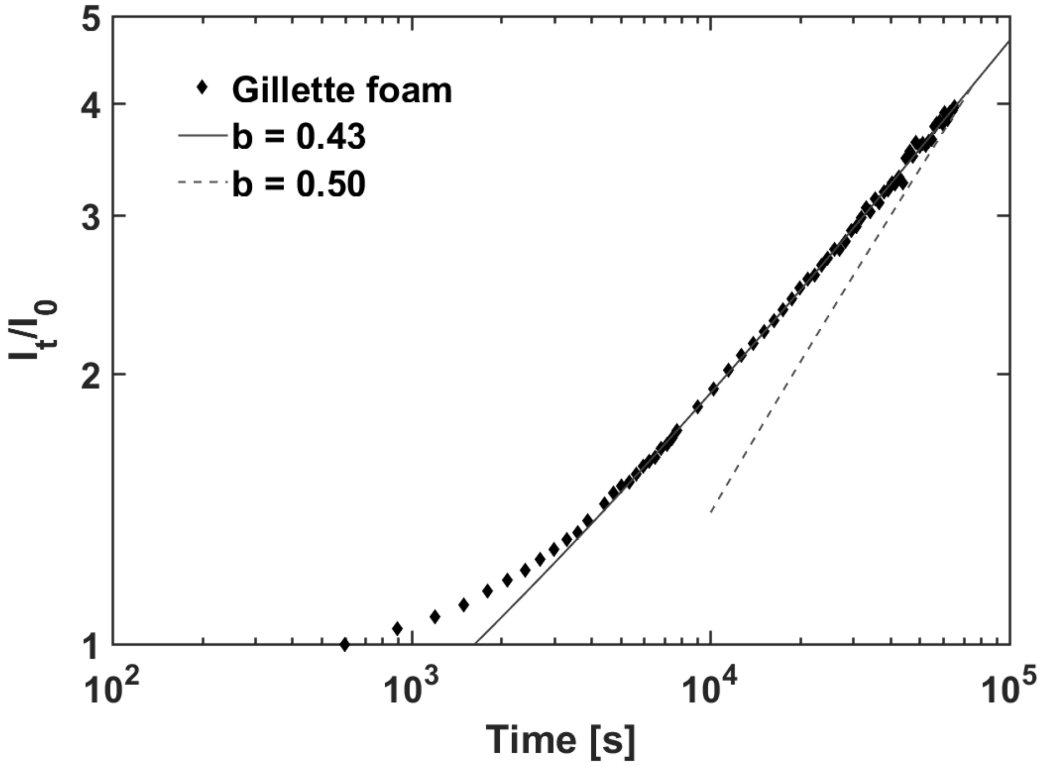

Figure 3.4: **Gillette foam coarsening.** *The graph shows the normalised transmitted intensity over time for the Gillette foam sample, that corresponds to the trend of the normalised mean bubble radius growth. The dashed line has slope 0.50 as the theoretical prediction for a dry foam. The continuous line represents the fitting curve* $y = a \cdot t^b + c$ *obtained by interpolating the data showing the self-similar behaviour. The exponent* b *is found to be equal to 0.43* $\pm$ *0.05. Fit parameters are reported in table 3.2.*

Fitting curve: $y = a \cdot t^b + c$	
a	0.03 ± 0.02
b	0.43 ± 0.05
c	0.2 ± 0.3

Table 3.2: **Fit parameters.** *The table reports the parameters for the power law interpolation. The exponent value found for our Gillette foam sample b=0.43* $\pm$ *0.05 results compatible with the one found in literature, z=0.45* $\pm$ *0.05 [12]*

Foamed emulsions

In this section, we proceed with the study of 3D foamed emulsions, exploiting diffusing-wave spectroscopy. As stated previously, foamed emulsions bear two different kinds of scatterers: air bubbles and oil droplets. As the emulsions are stable on the timescale of the experiments, we can assume their contribution to the total scattered intensity to be constant in time.

We first prepared a suitable volume of emulsion, approximately 250 ml, at the desired oil fraction. Foam was then generated with the kitchen mixer and, after 30 minutes of mixing at maximum speed, a square cell of side 8 cm and thickness 20 mm was carefully filled with foam with the aid of a spoon, paying attention not to include large air bubbles while filling and closing the cell. Then the foam sample was put over the laser beam in the DWS set-up, as shown in figure 2.5. The same procedure was repeated for emulsions at different oil fractions, ranging from 70% to 82%.

As already done with Gillette foam, we acquired and averaged the transmitted light intensity over proper time intervals. We report in figure 3.5 two examples of intensity detected during different time intervals for a foamed emulsion of ϕ=80%. The graph on the left shows the intensity over a shorter time range than the one on the right, since the former corresponds to the beginning of the experiment while the latter to the end, when we expect coarsening to have a slower rate.

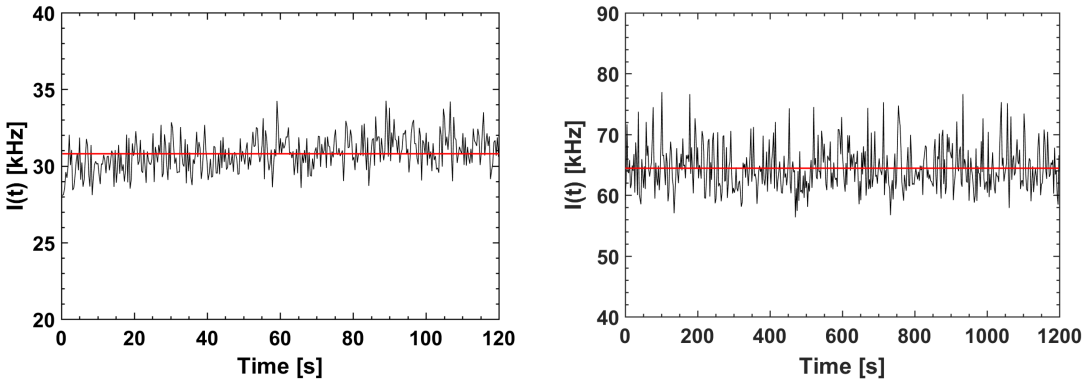

(a) (b)

Figure 3.5: **Intensity over different time intervals.** *We report an example of intensity samples for a DWS experiment for a foamed emulsion having 80% of oil fraction. Figure (a) shows the transmitted light intensity over the first 120 s long time interval. Mean value (31 ± 1) kHz. Figure (b) shows the intensity detected during the last 1200 s long time interval of the same experiment, which is longer since the foam coarsening is expected to have a slower rate. Mean value (64 ± 4) kHz.*

Since the transmitted light intensity depends on many experimental factors, like the laser power, the assorbance of the filters and the foam sample thickness, it is not meaningful to compare the outcome intensities as they are, for different experiments in different experimental conditions. Once again we can renormalise the mean intensity trends for different experiments, as shown in figure 3.6.

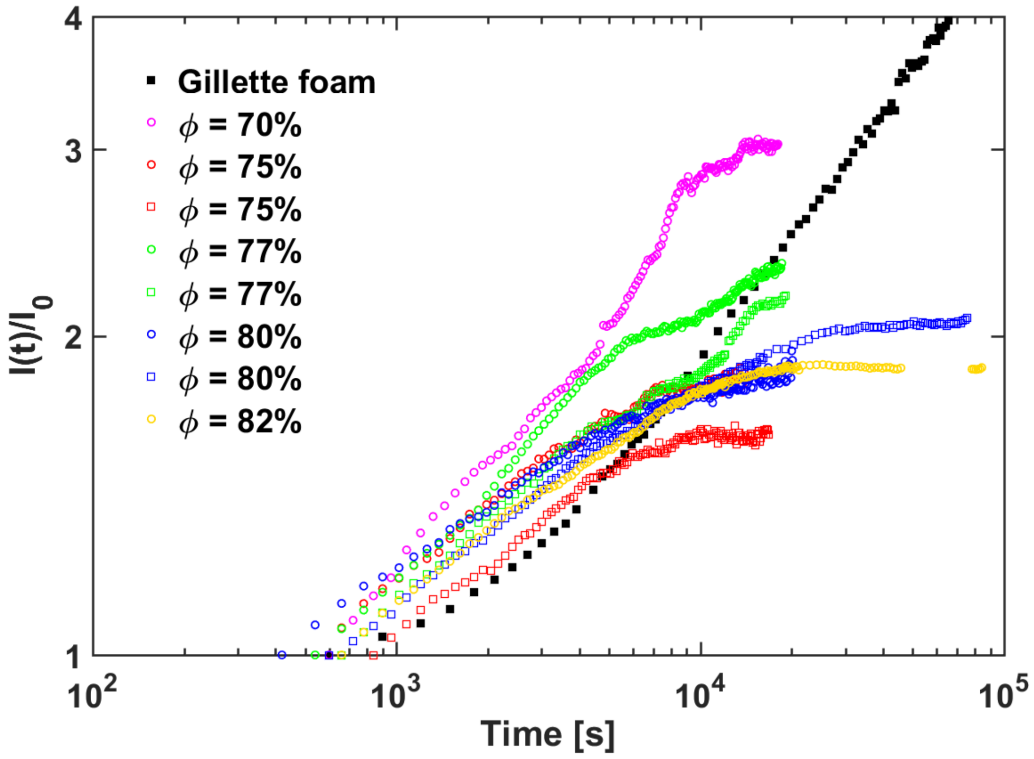

Figure 3.6: **Foamed emulsions.** *The plot displays the time evolution of normalised intensity for foamed emulsions at different oil fractions ϕ. The Gillette foam curve is also reported for visual comparison. For some oil fractions, we carried out two measurements for two different foam samples in the same experimental conditions to check the reproducibility of the results. One can see that after some time almost all the curves start flattening. Although these curves reproduce the time evolution of the mean bubble radius inside the foam sample, they do not give information about the actual size of the radii. These curves need to be scaled.*

Data in figure 3.6 show that foamed emulsions globally evolve in a very different way than Gillette foam, whose evolution is reported as well for visual comparison. Let us start by observing that some curves seem to flatten after few hours, while some others keep on growing, but they are all much less smooth than the Gillette one. For example, we can see that the curve corresponding to ϕ=70% rises much more than the curves at higher oil fractions, showing a step only once the intensity almost triples its initial value.

By contrast, the plateau is clearly evident at ϕ=80%, where the curve smoothly start flattening after five hours, and at ϕ=82%, where the curve seems to stay constant for very long time.

As we know there is a proportional relation between the intensity and the mean bubble radius, a plateau on the intensity curve could mean that after some time the average bubble size stops increasing or its growth is markedly slowed down. However, since the intensity curves are normalised, they correspond to the evolution of the normalised mean radius. If we really aim to understand what happens to our foamed emulsions as they coarsen, we need to find a way to rescale the curves in figure 3.6 to get the dimensional mean bubble radius growth over time.

As already explained in §2.3.2, we used the 3D foam pictures acquired at the end of each DWS experiment, to get a rough estimate of the final bubble size. The rescaling of the curves was achieved by employing the following relation:

$$\langle R(t)\rangle = \frac{I(t)}{I(t_f)} \cdot \langle R(t_f)\rangle \tag{3.1}$$

where $I(t_f)$ is the final averaged intensity corresponding to the last time interval of the experiment, while $\langle R(t_f)\rangle$ is the mean bubble radius of the foam sample at the end of the DWS experiment, obtained with the Matlab program, as already shown in figure 2.6.

The result of this procedure is shown in figure 3.7, where one can see how the curves display a plateau at radius values between 700 μm and 900 μm. One can intuitively expect that the more elastic the emulsion inside the foam, the more the coarsening should be hindered, reaching a smaller saturation mean bubble size.

We can see that this time the sample thickness of 20 mm is not always much larger than the average bubble size (the minimum value is around 20 bubbles across). However, the diffusion limit is ensured by the presence of the emulsion oil droplets dispersed in the Plateau borders, whose light scattering contributes to randomise the photon paths. Hence we are still within the validity of diffusion-wave spectroscopy.

It is necessary to remember that the method used for calculating the bubble radius from 3D foam pictures is not very accurate. This causes a large error on the absolute values of the mean bubble radii, but not on the size evolution, whose error comes from DWS intensities and results smaller. The maximum error from the image treatment was roughly evaluated as explained in §2.3.2 and results approximately the 30% of the mean bubble radius.

Thus, even if DWS provides an accurate trend for the bubble growth, the scaled curves in figure 3.7 eventually depend on the absolute values of the bubble radii, which have a large margin of error. As the error bar is meant only on the absolute value of the mean radius, not on its trend over time, the real curves in figure 3.7 may probably shift along the vertical axis, within their error bars.

Before concluding this section, let us discuss a little about these first results. What we observed is a slowing down of foam coarsening, which seems to almost halt in foamed emulsions having high concentrations of oil droplets.

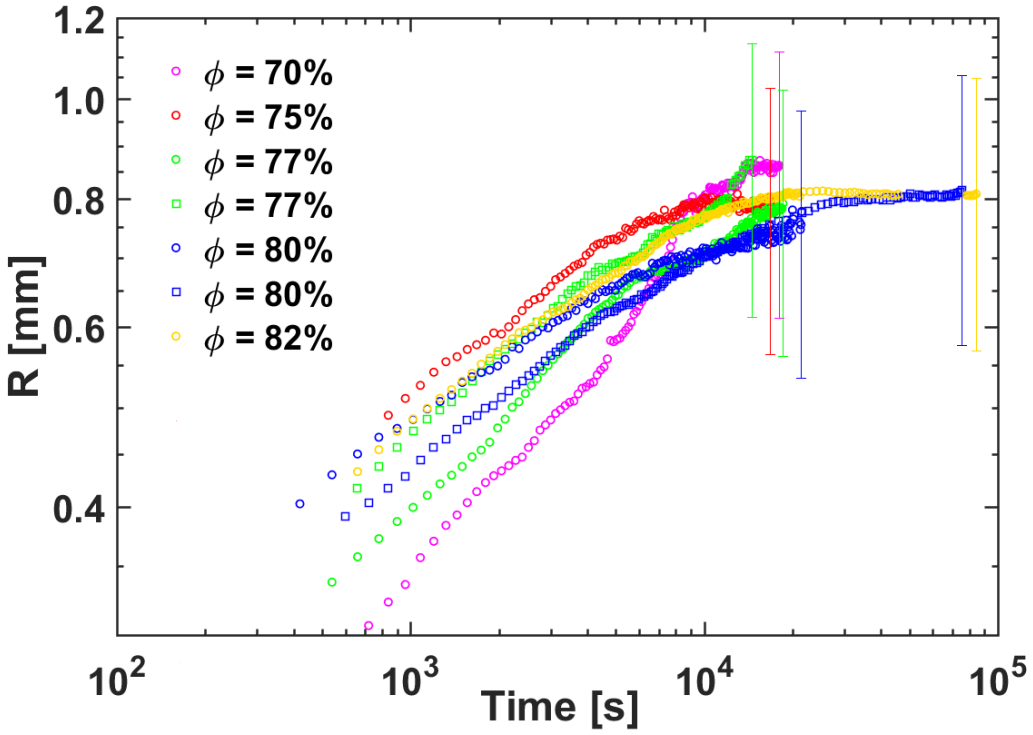

Figure 3.7: **Foamed emulsions.** *The plot shows the time evolution of the mean bubble size, obtained by rescaling the DWS curves in figure 3.6 by analysing the 3D foam pictures at the end of each experiment, as explained in §2.3.2. Here one can see that the curves become nearly flat at bubble radii which are all within the error bars. The large error bars come from the image treatment and are meant only on the absolute value of the mean radius, not on its evolution.*

We know from the literature [23] that coarsening can be inhibited when the yield stress of the continuous phase overcomes the Laplace pressure between neighbouring bubbles. We have seen in §3.1 that our emulsions display a storage modulus which spans values between 10 Pa and 100 Pa, but the yield stresses are much smaller, less than 1 Pa. Knowing that the surface tension is around 29 mN/m [33], as the radii of the bubbles increase up to values around 800 μm because of coarsening, the corresponding Laplace pressures decrease to values around 70 Pa which can result smaller than the emulsion G' for some foam samples, but not smaller than the emulsion yield stress. However, the large margin of error on the absolute values of the final mean bubble radii does not allow us to conclude more with certainty.

Some recent results in the literature [3] suggest that the yield stress of the total foam should be considered, instead of the yield stress of the continuous phase. Unfortunately, we did not have the possibility to perform rheology tests on foamed emulsions, as these results arrived once we had no more rheometers available. Then we could not measure the yield stress of our foams.

We also observed from our data that the coarsening rates are quite slow compared to Gillette foam. This may be due to a reduced permeability of the thin films between bubbles, which would impact on foam coarsening and make it slower, as seen in §1.3.3. In order to probe the film permeability in our systems, we performed 2D foam experiments, whose results are reported in §3.4. However, before switching to 2D foams, we report in the next section some comments about the 3D foam photographs taken.

3.3 Imaging

In this section we shall report the results obtained from the monitoring of 3D foams through imaging. In addition to qualitative information regarding the foam evolution, we are able to get an estimate of the mean bubble radius inside the foam samples from the image treatment, as already explained in §2.3.2.

Absence of drainage

No significant drainage has been observed during the experiments. Since we employed foam samples with thickness 20 mm for DWS experiments, we always checked visually both sides of 3D foam samples at the end of each experiment, in order to check if the foam was wetter on the bottom and dryer on the top. In figure 3.8 we report an example for one sample of foamed emulsion having oil fraction ϕ=80% and liquid fraction ϵ=10%. The two pictures were taken at the end of a DWS experiment, namely 22 hours after foam creation during which the foam sample remained static and was never turned upside down. One can see on the pictures that foam appears very similar on the top and on the bottom, without any significant liquid fraction difference after such long time. Thus, our choice to use emulsions as the continuous medium in foams to avoid drainage is experimentally justified.

Coarsening and negligibility of coalescence

The efficiency of the surfactant employed in our systems, should make coalescence negligible in the absence of significant drainage. As shown in the previous section, the latter is avoided thanks to the elasticity of the emulsions that constitute the continuous phase of our foams. In order to ensure that coalescence is actually negligible, we took sequences of pictures at constant frame rates for each foam studied with diffusing-wave spectroscopy. After foam generation, we filled two different samples, one of thickness 20 mm for DWS and another one of thickness 10 mm for imaging. The latter is thinner in order to have enough transmitted light for image creation.

In tables 3.3 and 3.4 we report some pictures at different times after foam creation. No significant coalescence is observed in the images, as this would result in a very uneven size distribution. Therefore we can assume that the intensity evolution measured using DWS is indeed linked to coarsening. The typical appearance of foam coarsening is

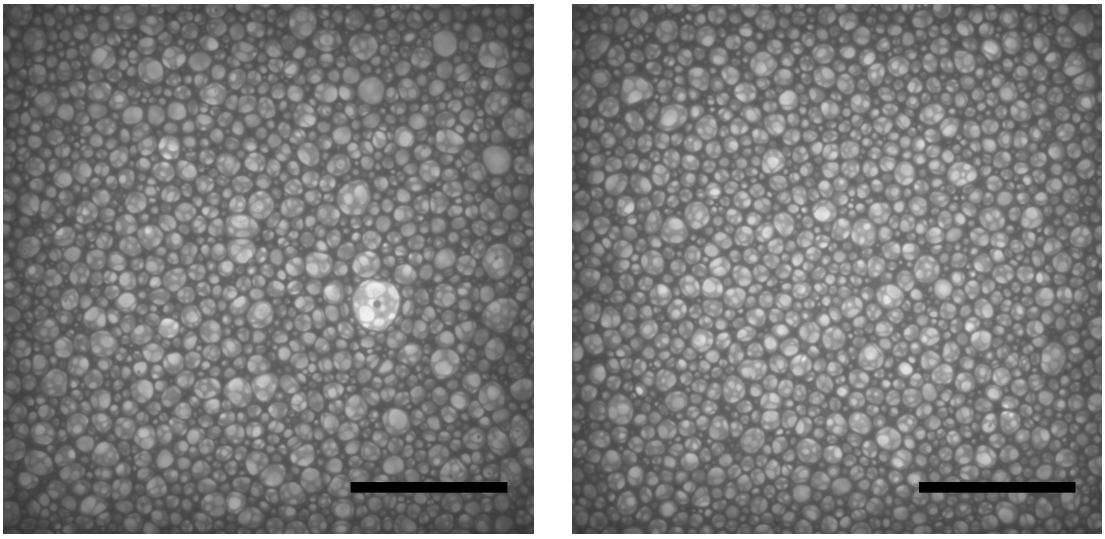

(a) (b)

Figure 3.8: **Negligible drainage.** *We report the pictures of the top (a) and of the bottom (b) of the same sample filled with a foamed emulsion of ϕ=80% and ϵ=10%. The sample thickness is equal to 20 mm and the pictures were taken 22 hours after foam generation. As one can see, the two pictures appear very similar, without displaying any significant difference in the liquid fraction, confirming that drainage is negligible at such high oil fractions. Scale bars 20 mm.*

observed for each foam sample: as one can see from the pictures, large bubbles slowly grow at the expense of tiny ones which gradually disappear, leading to an increase of the average bubble size. Let us now compare the evolution of foams having different oil fractions in the continuous phase. Comparing the mean bubble size at the same instant in different samples, it seems to monotonically decrease as ϕ increases, except for the two samples having ϕ=75% and ϕ=77%, for which the bubbles appear slightly bigger for the latter. After five hours, it is visually clear that the mean bubble size in the ϕ=70% sample is much bigger than in the ϕ=82% one.

We have already explained the advantages of using spectroscopy instead of imaging for studying foam coarsening. However, we can use these photographs to further check the validity of DWS results. We can analyse some of the pictures with the same Matlab program used for scaling DWS curves, to get the trend of the average bubble radius over time also with this method.

The result of this procedure is reported in figure 3.9. We consider two experiments of foamed emulsions at ϕ=80%, performed in the same experimental conditions. The same color indicates that the same foam was used to fill two different samples, one of thickness 20 mm for DWS and one of 10 mm for imaging. This way we can follow simultaneously the bubble size evolution inside the two samples with two different methods. We can see that pictures confirm the plateau obtained with DWS.

There is a vertical shift between the curves corresponding to simultaneous experiments, although we used the same Matlab program for image treatment. This shift can be due to the different confinement of bubbles inside cells of different thickness. However, the vertical shift between the two methods is not much different from the one between two different experiments, suggesting that this shift is all linked to the errors of the measurements.

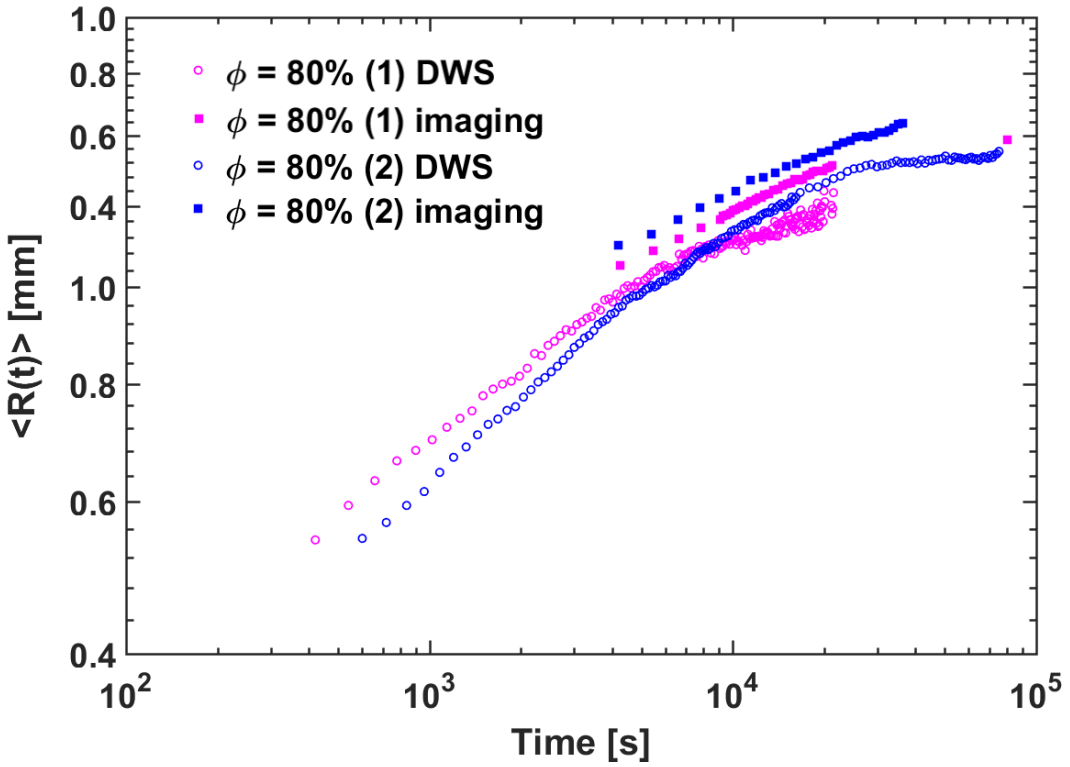

Figure 3.9: **DWS vs imaging.** *The plot shows the results of two experiments for foamed emulsions at ϕ=80% in the same experimental conditions. We use the same color to follow the ageing of the same foam inside two different samples. The bubble size evolution built directly from pictures follows the same trend found with DWS. The shift between the curves is probably due to the different confinement of the foam inside the two samples of different thickness and to the error linked to image treatment.*

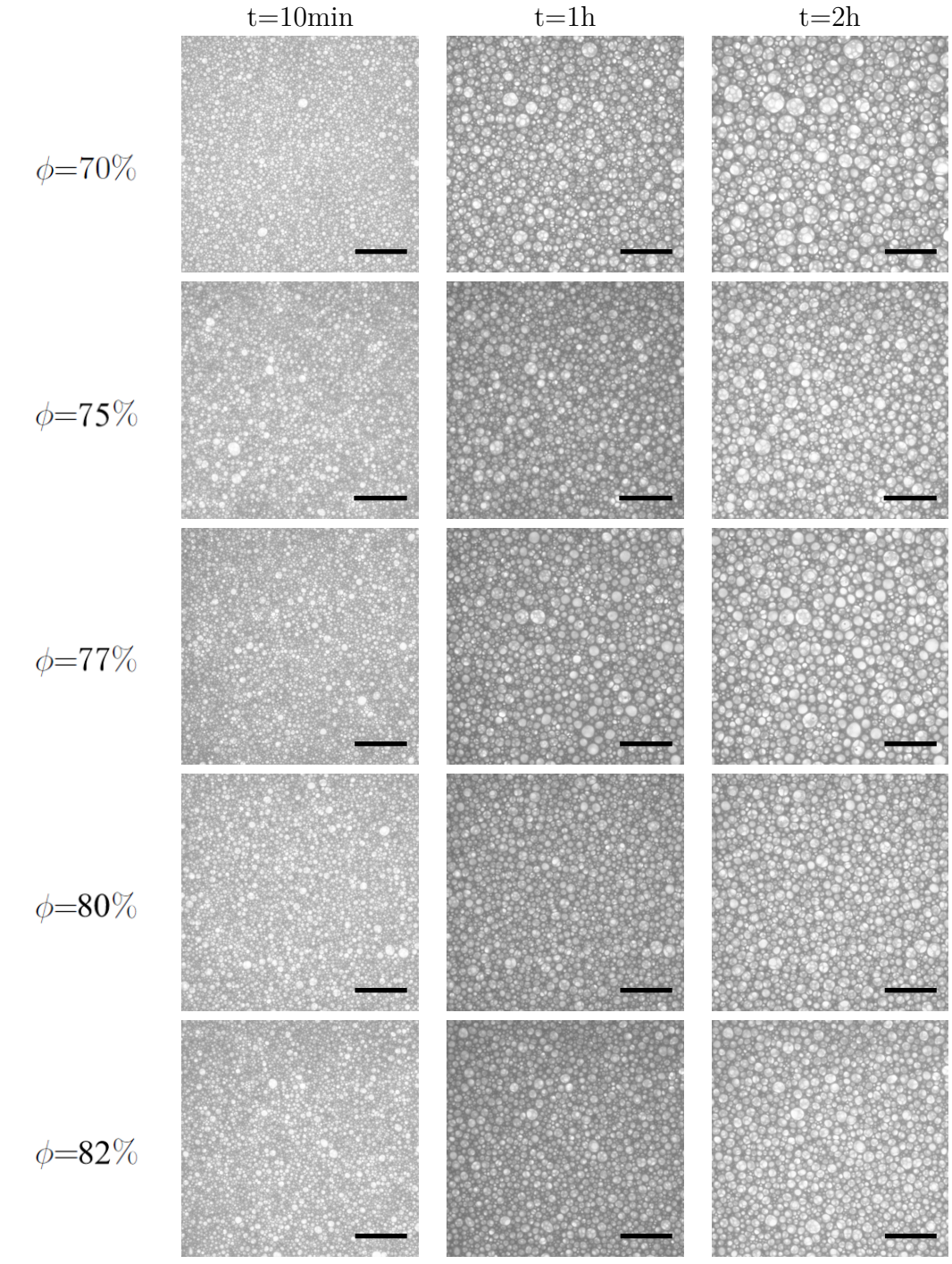

Table 3.3: **3D foam coarsening.** *The table reports a first extract of pictures of foamed emulsions evolution. Each row shows one foam sample at different instants and one can observe that as the time after foam creation increases, the mean bubble size grows because of coarsening. Following a column one can compare the appearance of foams having different oil fractions at the same instant. The bubble size seems to monotonically decrease as ϕ increases. Scale bars 20 mm.*

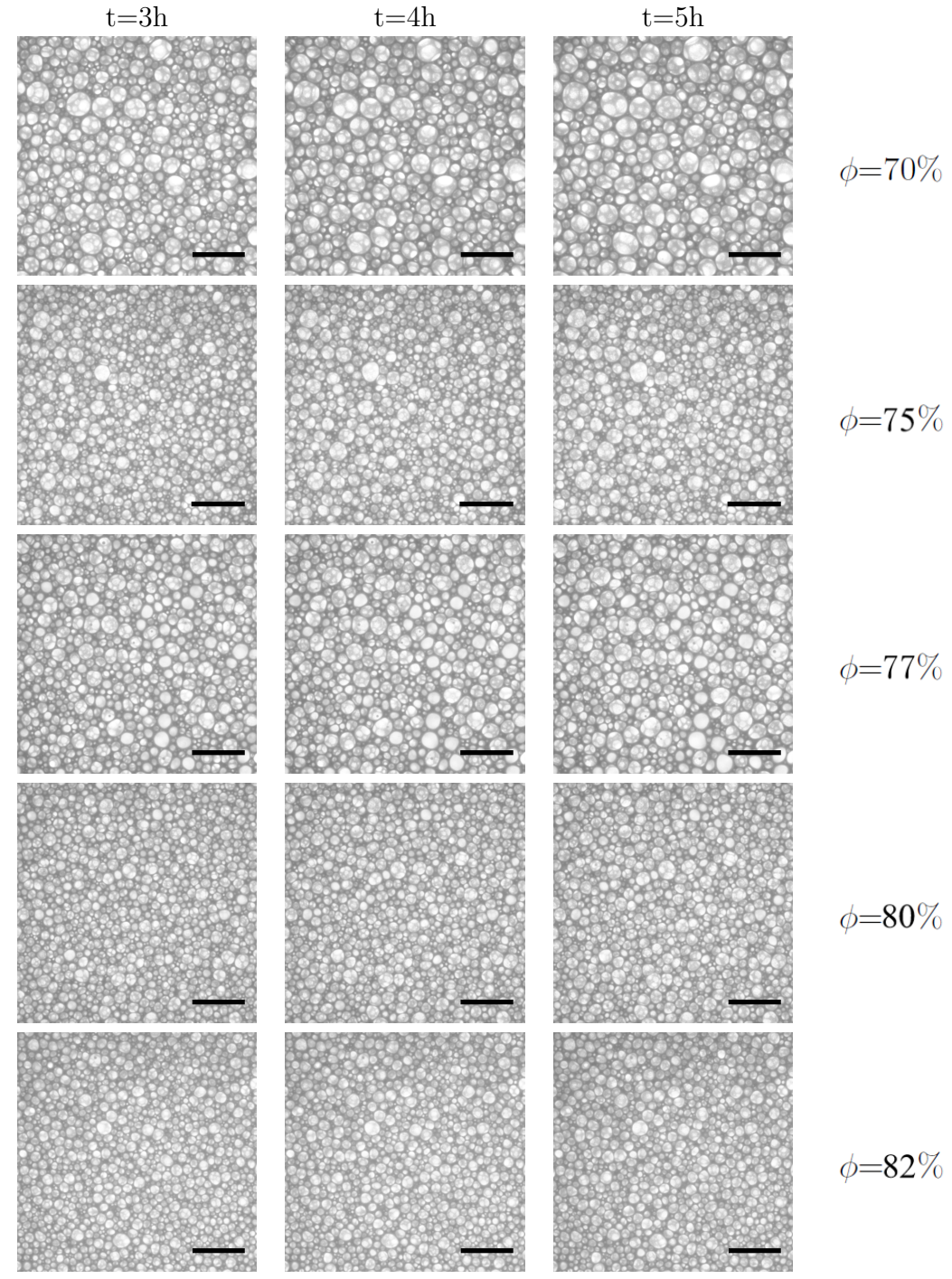

Table 3.4: **3D foam coarsening.** *Here is a second extract of pictures of 3D foamed emulsions. Each row shows the typical growth of the mean bubble size of one foam sample over time. Following a column one can compare the appearance of foams having different oil fractions at the same instant. The bubble size decreases as ϕ increases: after five hours, it is visually evident that bubbles in the ϕ=70% sample appear much bigger on average than the bubbles in the ϕ=82% one. Scale bars 20 mm.*

3.4 Film permeability

We know that foam coarsening is driven by the gas diffusion through the liquid phase between bubbles of different sizes. In quite dry foams, like the ones we are considering, the gas will permeate mainly through the thin films between neighbouring bubbles, as the Plateau borders are much thicker. Thus, this mechanism strongly depends on the liquid film permeability.

In order to estimate this relevant parameter for our systems, we carried out 2D foam experiments. We know that coarsening depends on film permeability through the effective diffusion coefficient D_{eff}, which appears in the Von Neumann's relations already discussed in §1.3.3.

We know from equation (1.9) that D_{eff} is related to the rate of gas diffusion D_f and to several other parameters, such as the Henry coefficient, which takes into account the solubility of the gas in the liquid, the surface tension of the gas/liquid interface, the film thickness and the foam liquid fraction.

Once again, we first start presenting the results obtained for a standard stable foam already studied in the literature. Then we report the results and the complications we ran into while studying foamed emulsions in two dimensions.

Fairy foam

First of all we repeated an experiment already done in the literature with the same set-up [32]. We studied coarsening in a pseudo-2D foam made with an aqueous solution of Fairy Original washing-up liquid. The exact chemical composition of Fairy is unknown: the label states only that it contains 15-30% of anionic surfactants, 5-15% of non ionic surfactants and other additives. Fairy foam is characterised by a strong stability of thin liquid films, which allows to verify Von Neumann's relations in 2D without observing coalescence.

The 2D foam was created by injecting air bubbles from the bottom of the reservoir shown in figure 2.8. Air was injected through a needle connected to a syringe previously filled with air, which was pushed at a constant rate by a compressor. If the gas flux is slow enough one can get a foam which is in good approximation monodisperse. The dimension of the bubbles can be adjusted by properly choosing the needle diameter. The liquid fraction depends on the height of the liquid inside the reservoir, which was mantained at atmospheric pressure by a small tube in contact with air.

Since the foam was constantly in contact with the liquid inside the reservoir, the excess of liquid could drain during 2D foam coarsening, meaning that the liquid fraction was not kept constant during this kind of experiment. What remained constant with this set-up configuration is the capillary pressure.

We studied 2D foam coarsening by taking pictures at a constant frame rate. Some of them are reported in table 3.5. The foam is in good approximation monodisperse at the beginning, resembling an ordered crystalline structure. After the onset of coarsening, the polydispersity start growing and the average bubble size visually increases. The typical behaviour predicted by Von Neumann's laws is observed: the relevance of

topology becomes evident after few hours. The bubbles with five neighbours or less start decreasing over time and slowly disappear, while bubbles with seven neighbours or more keep on growing. This leads to a decrease of the total number of bubbles and to an increase of the mean area of the remaining ones, both typical features of foam coarsening. In figure 3.6 we can see a focus on a five-sided bubble which is reducing its area while passing its gas to the surrounding bigger bubbles, according to equation (1.8).

By analysing these pictures using the already mentioned custom made Matlab program [14], we can recognise all the bubbles on the picture and get all the information about their size, their position and their number of neighbours over time. First of all, we can follow the total number of bubbles over time, that we can compare with the trend found in [32]. The plot is reported in figure 3.10.

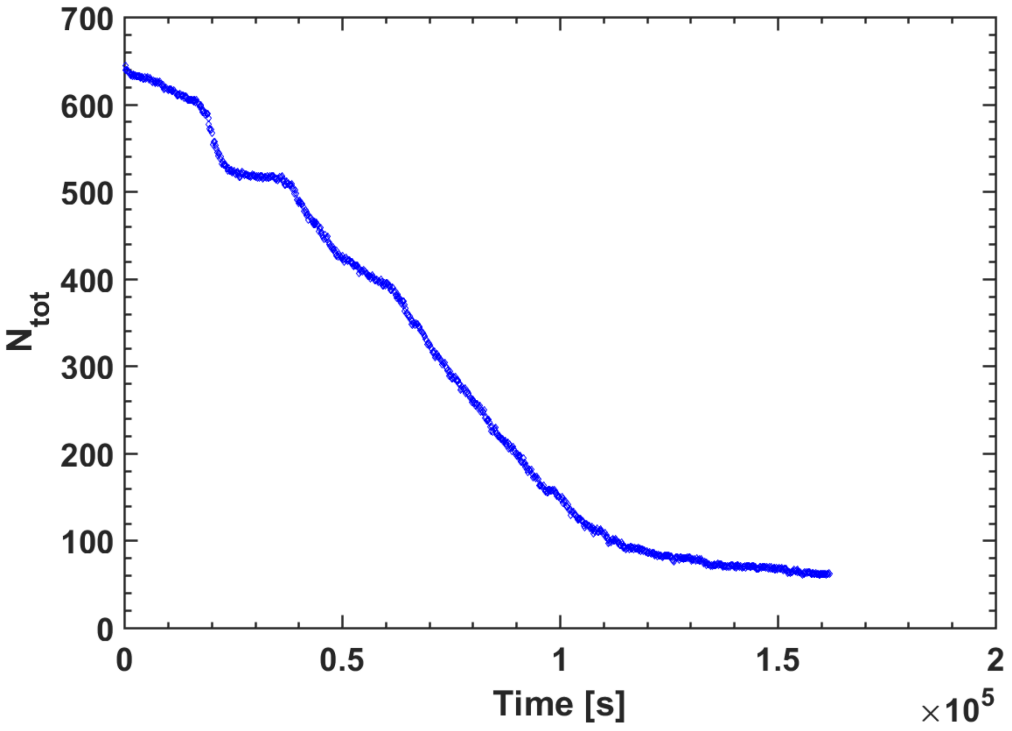

Figure 3.10: **Total number of bubbles.** *The plot reports the total number of bubbles over time. As expected N_{tot} decreases. The steps are a characteristic feature of a quasi-monodisperse foam, where the five-sided bubbles of equal size disappear at the same instant. In our case N_{tot} is not constant at the beginning because of a movement of bubbles inside the 2D cell, which does not affect the next results.*

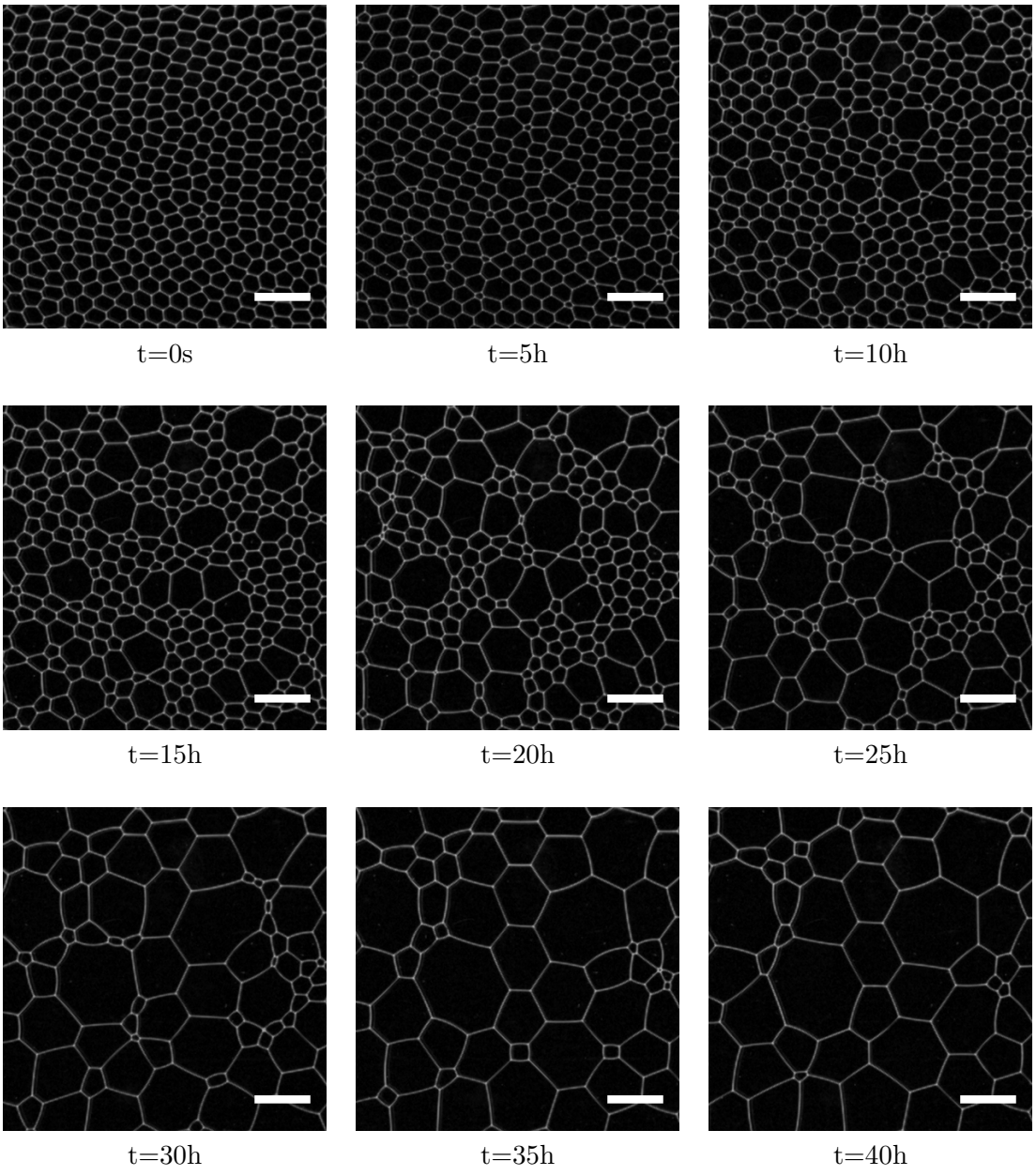

Table 3.5: **Fairy foam coarsening.** *The table reports some of the photographs taken of the 2D foam made of Fairy liquid, which coarsens over time. The bubbles are initially monodisperse at t=0 s and their size increases over time. After five hours one can see that five-sided bubbles start visually decreasing, while the bubbles with more than six neighbours become bigger. Scale bars 20 mm.*

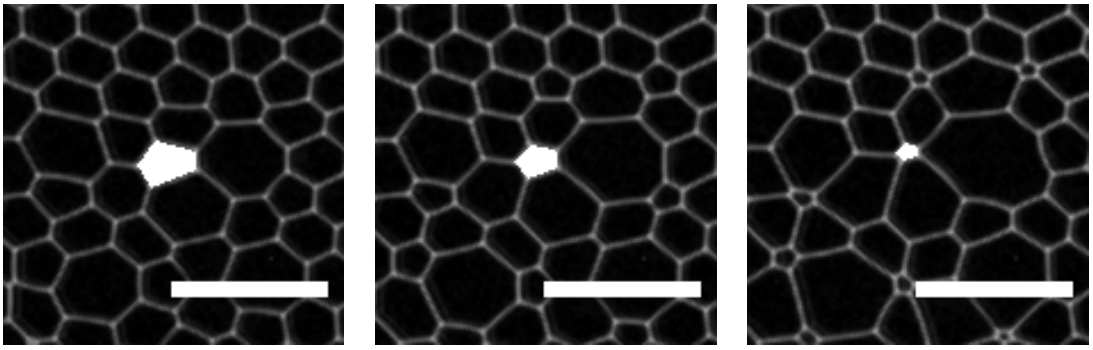

t_0 $t_0 + 2.5h$ $t_0 + 5h$

Table 3.6: **Disappearance of a bubble.** *The three pictures show a five-sided bubble (painted white) at different instants. After 2.5 hours it has already passed much of its gas to the surrounding bubbles. After 5 hours it is about to disappear. Scale bars 10 mm.*

Since we started by an approximately monodisperse 2D foam, we expected the total number of bubbles to be constant at the beginning. It should not vary until the disappearance of the first five-sided bubbles, which should occur simultaneously if the size of the bubbles is initially homogeneous. The instant of time at which this occurs is called *catastrophic time*. In our case, in figure 3.10 we observe a slightly decreasing slope instead of a constant value of N_{tot}. Our 2D foam was not perfectly monodisperse, but this slope is mainly due to the fact that we registered a little temporary shift of bubbles towards the reservoir at the beginning of the experiment, which stabilised by itself in a short time. However, it causes a loss of few bubbles since the beginning, because the Matlab program does not consider bubbles on the boundaries, and as soon as the bubbles move towards an edge of the picture, they are cut and no more taken into account. This explains the existence of that unexpected slope, which however does not affect further our analysis.

In fact, in order to get the diffusion coefficient, we are interested in the variation of the mean area of the bubbles with five and seven neighbouring bubbles respectively. We can consider the following relation for a group of n-sided bubbles:

$$\frac{\langle A_{n,t}\rangle - \langle A_{n,0}\rangle}{\langle A_{n,0}\rangle} = \frac{\pi}{3} D_{eff}(n-6)t \tag{3.2}$$

where $\langle A_{n,0}\rangle$ is the mean area of the n-sided bubbles at instant $t = 0$, $\langle A_{n,t}\rangle$ is its value at instant t and D_{eff} is the effective gas diffusion coefficient. Once obtained the trend of $\langle A_n\rangle$ from the pictures, it is immediate to get D_{eff}.

The normalised mean area evolution of n-sided bubbles is reported in figure 3.11 for n equal to 5, 6 and 7 respectively. One can easily see that the mean area of five-sided bubbles initially decreases, while the seven-sided ones have an area which is increasing in average from the beginning. By contrast, the mean area of bubbles with six sides is approximately constant, as expected.

Method of slopes

A focus on the first part of the graph is reported at the bottom of figure 3.11. Here we can see better how the two curves corresponding to n=5 and n=7 are linear and almost specular. By linearly fitting both of them with a curve $y = a_n \cdot t$ we can get the angular coefficients a_n for $n = 5$ and $n = 7$, which will have opposite sign. The coefficient D_{eff} is then obtained from a_n by using the following relation:

$$D_{eff} = \frac{3}{\pi} \frac{a_n}{n-6} \cdot \langle A_{n,0} \rangle \tag{3.3}$$

Results are summarised in table 3.7. We obtain D_{eff}=$(3.2 \pm 0.4) \cdot 10^{-4}$ mm^2/s from the evolution of five-sided bubbles and D_{eff}=$(3.8 \pm 0.4) \cdot 10^{-4}$ mm^2/s from the seven-sided ones. We note that the two values obtained are very close and their compatibility results 1.06. Moreover, they are of the same order of magnitude of the ones found in [32].

Method of slopes

	a_n [s^{-1}]	$\langle A_{n,0} \rangle$ [mm^2]	D_{eff} [mm^2/s]
n=5	$(-4.31 \pm 0.03) \cdot 10^{-5}$	7.7 ± 0.8	$(3.2 \pm 0.4) \cdot 10^{-4}$
n=7	$(+4.83 \pm 0.04) \cdot 10^{-5}$	8.3 ± 0.7	$(3.8 \pm 0.4) \cdot 10^{-4}$

Table 3.7: **Parameters.** *Effective diffusion coefficients measured through the method of slopes from the evolution of five and seven-sided bubbles. Intermediate parameters, namely the angular coefficient a_n and the initial mean area $\langle A_{n,0} \rangle$, are tabulated as well.*

Method of bubble tracking

We can get the coefficient D_{eff} in a different way, which will be useful later for studying 2D foamed emulsions. The Matlab program allows to follow the evolution of every single bubble. Hence we can calculate the D_{eff} by tracking the area variation of each bubble with n sides. By linearly fitting the single area variation with a curve $y = a_n \cdot t + b$ we can get the angular coefficient a_n, which is then averaged over the total number of bubbles having n neighbours. This is done in figure 3.12, which displays the results obtained for the coefficient a_n and its mean values, for bubbles having five and seven sides. According to Von Neumann's relation, we know that the angular coefficient a_n is essentially given by:

$$a_n = \frac{dA_n}{dt} = \frac{\pi}{3} D_{eff}(n-6) \tag{3.4}$$

hence we can directly get the effective diffusion coefficient D_{eff} from the relation:

$$D_{eff} = \frac{3}{\pi} \frac{a_n}{n-6} \tag{3.5}$$

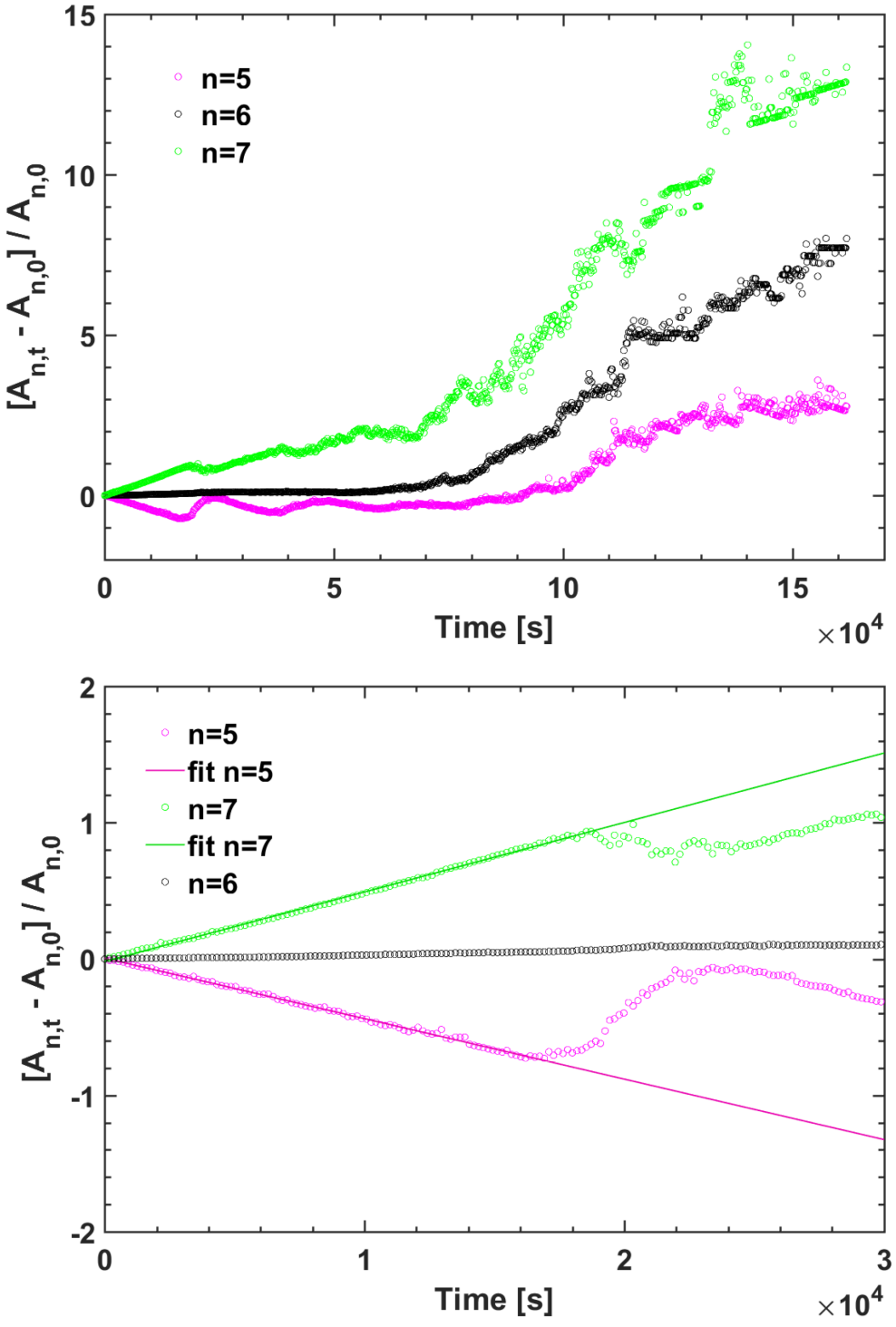

Figure 3.11: **Method of slopes.** *Picture on the top shows the time evolution of the normalised mean area for bubbles having different number of neighbours. Zooming on the first part, picture right below shows the two linear interpolations performed for n=5 and n=7 in order to get* D_{eff} *with the method of slopes.*

Results for a_n and D_{eff} are reported in table 3.8. We get D_{eff}=$(3.3 \pm 0.3) \cdot 10^{-4}$ mm^2/s by tracking single five-sided bubble evolutions and D_{eff}=$(3.7 \pm 0.5) \cdot 10^{-4}$ mm^2/s by tracking the seven-sided ones. We can note that these values are very close to the ones obtained with the previous method. Thus, this method proves reliable and results useful when measuring D_{eff} in polydisperse foams, like the ones we get by foaming emulsions with the mixer, as will be illustrated in the next section.

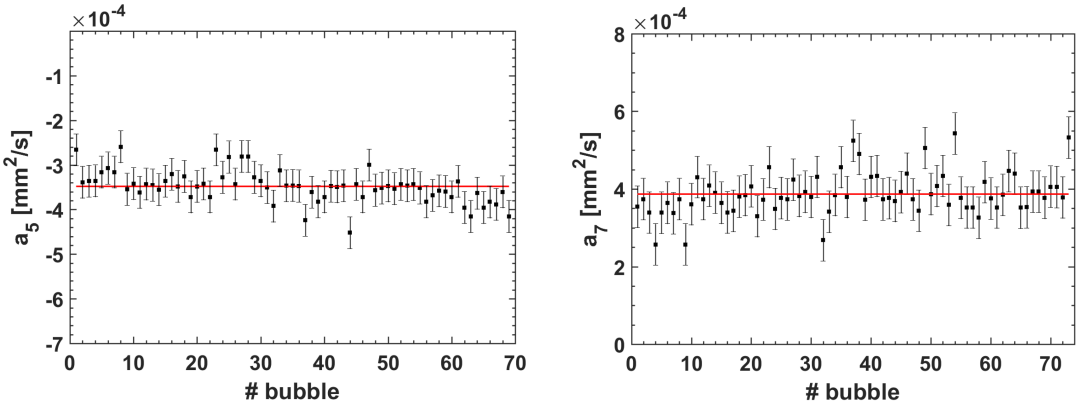

(a) (b)

Figure 3.12: **Bubble tracking.** *Picture (a) shows the angular coefficients a_5 found by tracking single five-sided bubbles. The horizontal red line represents the mean value $\langle a_5 \rangle = (-3.5 \pm 0.4) \cdot 10^{-4}$ mm^2/s. The same is done for bubbles with seven neighbours in picture (b), where the mean value is $\langle a_7 \rangle = (+3.9 \pm 0.5) \cdot 10^{-4}$ mm^2/s.*

Method of bubble tracking

	$\langle a_n \rangle$ [mm^2/s]	D_{eff} [mm^2/s]
n=5	$(-3.5 \pm 0.4) \cdot 10^{-4}$	$(3.3 \pm 0.3) \cdot 10^{-4}$
n=7	$(+3.9 \pm 0.5) \cdot 10^{-4}$	$(3.7 \pm 0.5) \cdot 10^{-4}$

Table 3.8: **Parameters.** *Effective diffusion coefficients D_{eff} measured by tracking single five and seven-sided bubbles. The mean values of the angular coefficients $\langle a_n \rangle$ are also reported in the first column.*

Foamed emulsions

The production of bubbles by air injection in emulsions at high oil fraction is not possible, because of their strong elasticity. If we try to inject air from the bottom, what we get is a single bubble which keeps on expanding until it reaches the surface and it bursts.

Therefore, we could not follow exactly the same procedure and we had to slightly modify the set-up configuration. We first created a 3D foamed emulsion by using the mixer, then we carefully spread it on the cell where then the joint was smaller so that the foam was no more in contact with the reservoir, which was left empty. Doing this, the liquid fraction, and not the capillary pressure, was kept constant during the experiment. The liquid fraction was measured before each experiment and was approximately the same as in the DWS experiments, namely around 10%.

Since the mixer produces a foam with very tiny bubbles, the foam in the cell was initially 3D even if we used the thinnest joint available, which has a thickness of 1 mm. A thinner joint would have probably allowed to get a monolayer of bubbles immediately, but the Matlab program [14] employed for processing the pictures would not have been able to recognise such small bubbles. Hence we always had to wait some time for the foam to age and become 2D, discarding the first sequence of pictures where the foam was still 3D. The time to wait for varies for each experiment, as it depends on the coarsening rate, and it oscillates between 2 hours for the minimum oil fraction and 9 hours for the maximum.

Once again, the evolution of the bubbles was recorded by taking photographs at constant time intervals, equal to 180 s. We repeated the experiment for foamed emulsions having different oil fractions, ranging from 70% to 82%. Some of the pictures are reported in tables 3.9 and 3.10. Before describing the evolution of the different samples in detail, we can already note that there is no clear sign of coalescence and it seems that foams age through coarsening only. As here we are working with a constant liquid fraction, unlike with the Fairy foam, the pseudo Plateau borders are getting thicker at the surface as the bubble size increases.

We can easily see from the pictures that the coarsening is strongly different than what we observed in Fairy foam. Let us start considering the foamed emulsion at ϕ=70%. We can see that the disappearance of small bubbles makes the average bubble size grow over time. However, we can see that the aspect of the bubble pattern is slightly different than the aqueous Fairy foam. This difference is enhanced when the oil fraction is increased. As time goes by, the bubble pattern changes until it does not even resemble a pattern of bubbles. It looks more like a pattern of solid grains. This peculiar ageing is clearly observed especially for foamed emulsions at ϕ=80% and ϕ=82%. The difference between the two samples at ϕ=70% and ϕ=82% can be better compared in figure 3.13, where we report an enlargement of two pictures after 68 hours.

	t=0s	t=6h	t=12h
ϕ=70%	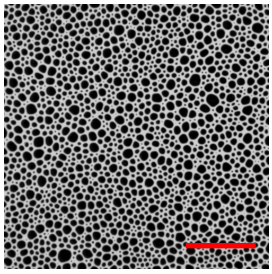	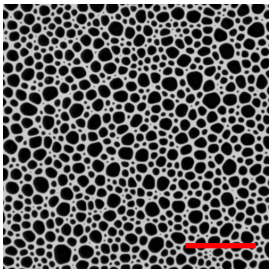	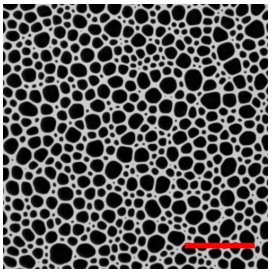
ϕ=75%	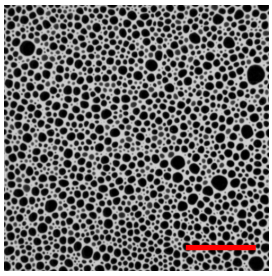	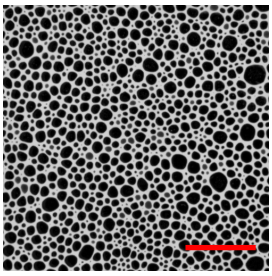	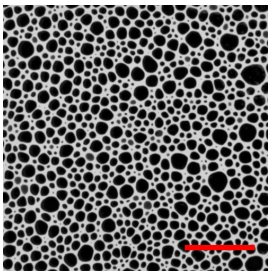
ϕ=77%	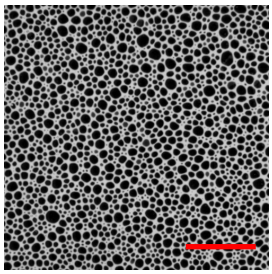	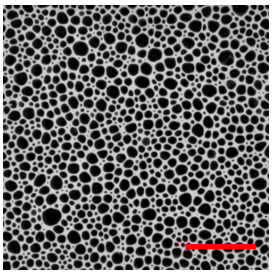	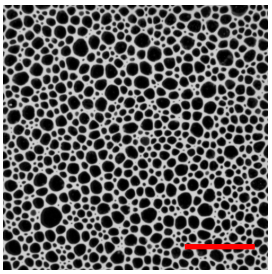
ϕ=80%	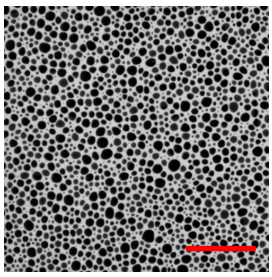	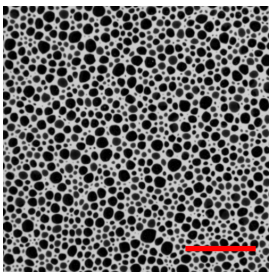	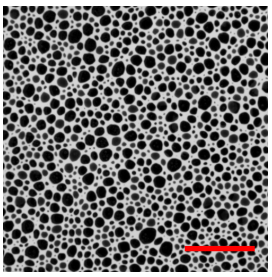
ϕ=82%	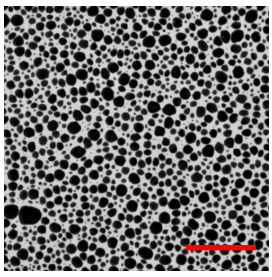	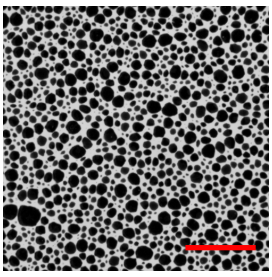	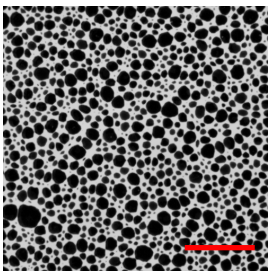

Table 3.9: **2D foamed emulsions.** *The table reports a first extract of pictures of 2D foamed emulsion evolution. Each row shows one foamed emulsion with a certain ϕ at different instants of time and one can observe the growth of the mean bubble size due to coarsening and the absence of coalescence. Following a column one can compare the appearance of foams having different oil fractions at the same time. Scale bars 20 mm.*

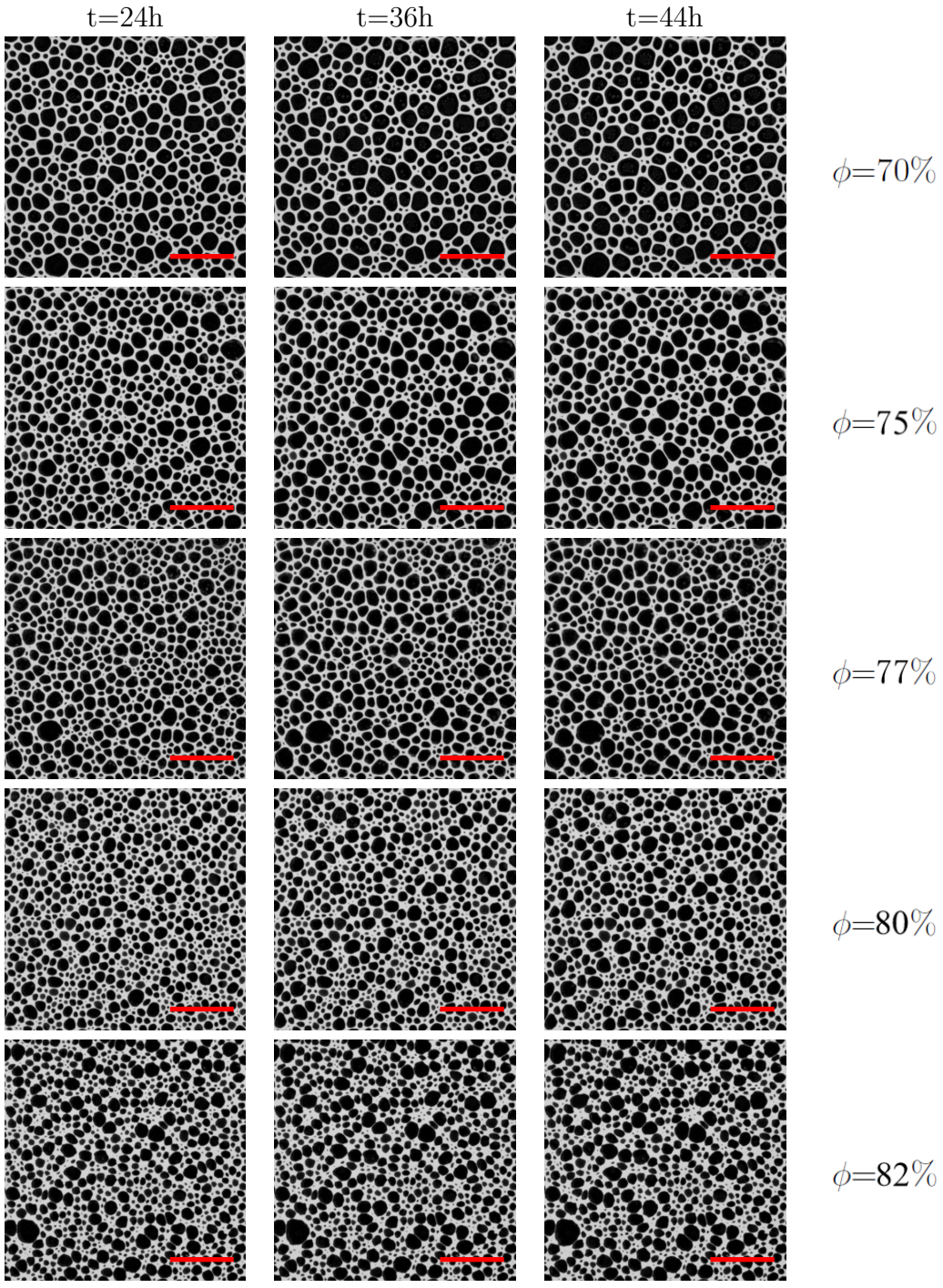

Table 3.10: **2D foamed emulsions.** *The table shows a second extract of image sequences for 2D foamed emulsions having different oil fractions ϕ. From the last column one can see that when ϕ is increased up to 82% the bubble appearance is totally different from the typical pattern observed for Fairy foam. The bubbles are not at all relaxed and the pattern looks like the evolution of solid grains instead of bubbles. Scale bars 20 mm.*

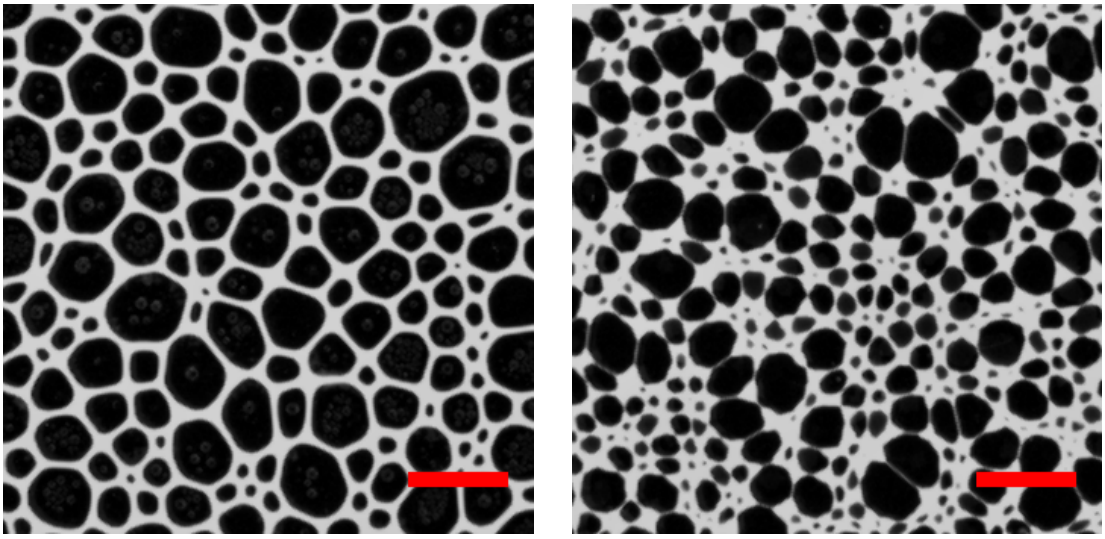

(a) (b)

Figure 3.13: **Comparison between ϕ=70% and ϕ=82%.** *The two figures show a zoom on the 2D foamed emulsions at ϕ=70% (a) and ϕ=82% (b) after 68 hours. One can observe that their appearance is totally different. The sample (a) still resembles a 2D foam, as one can still recognise the typical topology. By contrast, the sample (b) at higher oil fraction exhibits an amazing pattern where bubbles are not at all relaxed. The material really resembles the evolution of solid domains instead of bubbles. Scale bars 10 mm.*

The observed behaviour does not allow us to use Von Neumann's relation for 2D foam coarsening, since it is based on the topology of bubble pattern that here is completely different. What we can do is evaluating only the order of magnitude of the coefficient D_{eff} in such systems, by analysing some single bubbles for the foamed emulsion at 70% of oil, which is the only one that can be still considered as a foam.

Since we are now working with polydisperse foams, we use the method of bubble tracking as already done for Fairy foam. Instead of an initial interval of time, we consider an intermediate range where bubbles are a bit larger and the program can follow better the area evolution. Once again we interpolate the data with a linear curve $y = a \cdot t + b$. Figure 3.14 reports an example of linear fit for a single five-sided bubble. By repeating the same procedure for ten different five-sided bubbles and taking the weighted average, we can evaluate the mean angular coefficient $\langle a \rangle$, as displayed in figure 3.15, which results equal to $(-9.6 \pm 0.1) \cdot 10^{-5}$ mm^2/s.

By using the equation (3.5), we can get a rough estimation of the effective diffusion coefficient D_{eff}, which results equal to $(9.2 \pm 0.1) \cdot 10^{-5}$ mm^2/s. We can see that D_{eff} in foamed emulsions is smaller than the values found for Fairy foam, whose weighted average was $(3.4 \pm 0.2) \cdot 10^{-4}$ mm^2/s.

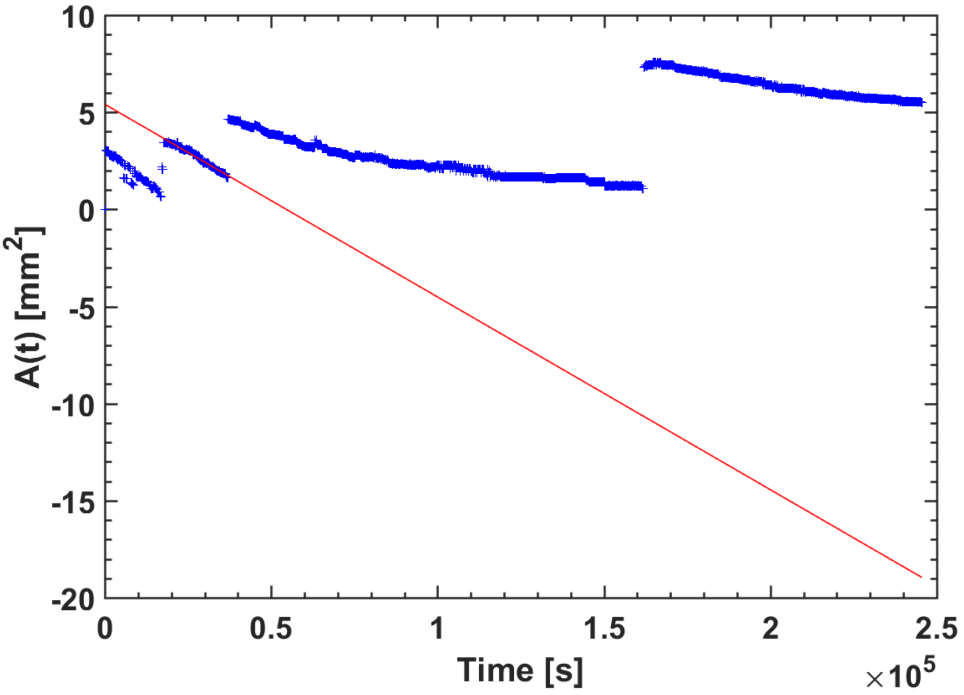

Figure 3.14: **Single bubble tracking.** *Example of bubble tracking. The plot shows the single bubble area over time. The fit is done on an intermediate time interval, where the Matlab tracking is more efficient. Every jump in the graph means that the considered five-sided bubble has disappeared and the Matlab program starts tracking a different five-sided bubble.*

In order to better understand the origin of this difference, we need to remind of what the coefficient D_{eff} depends on. Let us rewrite for the sake of convenience the equation (1.9) here below:

$$D_{eff} = D_f \, \frac{2\,He\,\gamma\,V_m}{h} \, a(\epsilon) \tag{3.6}$$

Let us now analyse each of the possible contributions, starting from a relevant observation about the 2D foam geometry. We know that D_{eff} depends on the liquid fraction via the geometric factor $a(\epsilon)$, that takes into account the effective area of gas transfer.

With Fairy foam we have worked with a constant capillary pressure, while the liquid fraction could vary during the experiment, as the liquid was free to drain into the reservoir. This way, as seen from the pictures in table 3.5, the pseudo Plateau borders remained quite thin and we can consider their radius r_{PB} to be much smaller than the spacing between the two plates e. Therefore, if $r_{PB} << e$ the effective height of the thin film e_{eff} is approximately equal to the spacing e, and the geometrical factor can be considered equal to one, $a = e_{eff}/e \simeq 1$.

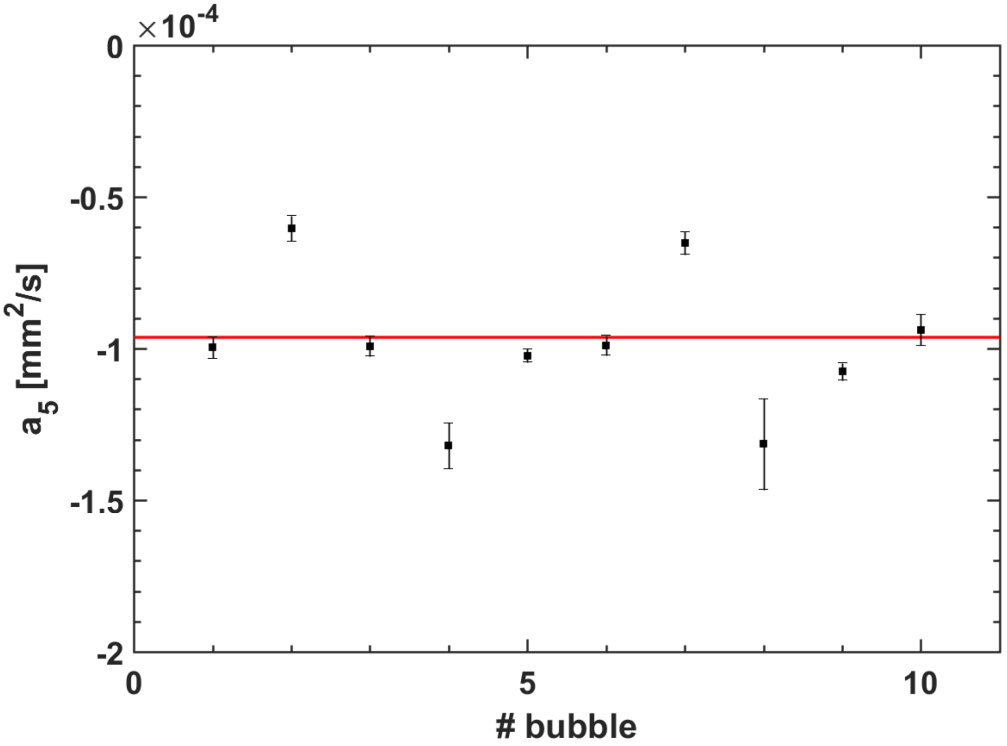

Figure 3.15: **Angular coefficients.** *The plot shows the angular coefficients a_5 obtained following the area variation of 10 different five-sided bubbles. The red line represents the weighted average equal to* $(-9.6 \pm 0.1) \cdot 10^{-5}$ mm^2/s.

For foamed emulsion this is not true, since the liquid fraction was kept constant during the experiments. We observed that the pseudo Plateau borders increase their thickness as the foam coarsens, and they are generally thicker than the ones in Fairy foam. The approximation done for Fairy results no longer true, as the effective surface through which gas diffuses from bubble to bubble can be smaller than the spacing between the plates, resulting in a geometrical factor smaller than one. Knowing that the liquid fraction of our foamed emulsion of ϕ=70% was equal to ϵ=9%, if we use the equation (1.10) we find a factor $a(\epsilon) = 0.5$.

Surfactants affect the D_{eff} directly via the surface tension γ. We know that the surface tension of Fairy liquid is equal to 27 mN/m, while the surface tension in emulsions with rapeseed oil and SDS results around 29 mN/m at oil fractions up to 70% [33]. The similarity between these two values suggests that the difference in D_{eff} should lie in the other involved parameters.

Let us now take into account the chemical composition of our foams. The film permeability k, which is given by the ratio:

$$k = RT\frac{D_f He}{h} \tag{3.7}$$

can be easily calculated from the coefficient D_{eff} and results around 3.5 $\cdot 10^{-7}$ m/s.

The Henry constant He depends strongly on the chemical composition of both gas and liquid phases. Even though there are no values in the literature for the Henry constant specifically for air in rapeseed oil, the solubility of air in other vegetable oils seems to be higher than in water. A higher He would lead to a faster coarsening, therefore we can say that the slowing down of the coarsening process is not linked to He, as it varies in the wrong direction. Table 3.11 shows some of the values for the Henry constants of the main air compounds in water and in some oils.

Henry constants

	Water [31]	Sunflower oil [7]	Corn oil [1]	Cottonseed oil [1]	Soybean oil [1]
N_2	0.0006	-	0.0028	0.0027	0.0038
O_2	0.0013	0.0057	-	-	-

Table 3.11: **Air solubility.** *The table shows the values found in the literature for the Henry constant He of nitrogen and oxygen in water and in other vegetable oils at T=25^{o}C. The values are all expressed in mol $L^{-1}bar^{-1}$.*

It is generally assumed that the diffusion coefficient D_f of the gas in the liquid film is equal to that in the bulk liquid, and therefore independent of the film thickness h. By contrast, it is inversely proportional to the molecular viscosity of the liquid. More precisely it is linked to the viscosity of water and oil separately, not to the emulsion viscosity, as the gas molecules do not feel the emulsion droplets as obstacles. As the viscosity of oil is higher than the one of water, if there are oil droplets within the films we expect D_f to be smaller.

Finally, the effective diffusion coefficient can be influenced by either the film thickness or a factor linked to the permeability of the interfaces. However, the latter is already taken into account by the surface tension. The film thickness h, which is fixed by the disjoining pressure, can play a fundamental role. A thicker film would decrease the permeability, and from the D_{eff} equation we can see that the thicker the films, the slower the coarsening.

In addition to all these qualitative comments, which open up to further future investigations, we observed that coarsening is actually influenced by the viscoelasticity of the continuous phase. What we observed is that increasing the storage modulus G' of the emulsion, namely increasing its elasticity, the system evolves in a way that does not resemble the ageing of a traditional 2D foam.

Let us now compare the foamed emulsion behaviour at different oil fractions. Since applying Von Neumann's laws to foamed emulsions at higher ϕ is not meaningful, we are not able to get the variation of D_{eff} with ϕ. Anyway, what we can do is to count the total number of bubbles over time for different foamed emulsions and see if something changes with ϕ. What we get is shown in figure 3.16, where we compare the normalised total number of bubbles N_{tot} for different oil fractions ϕ.

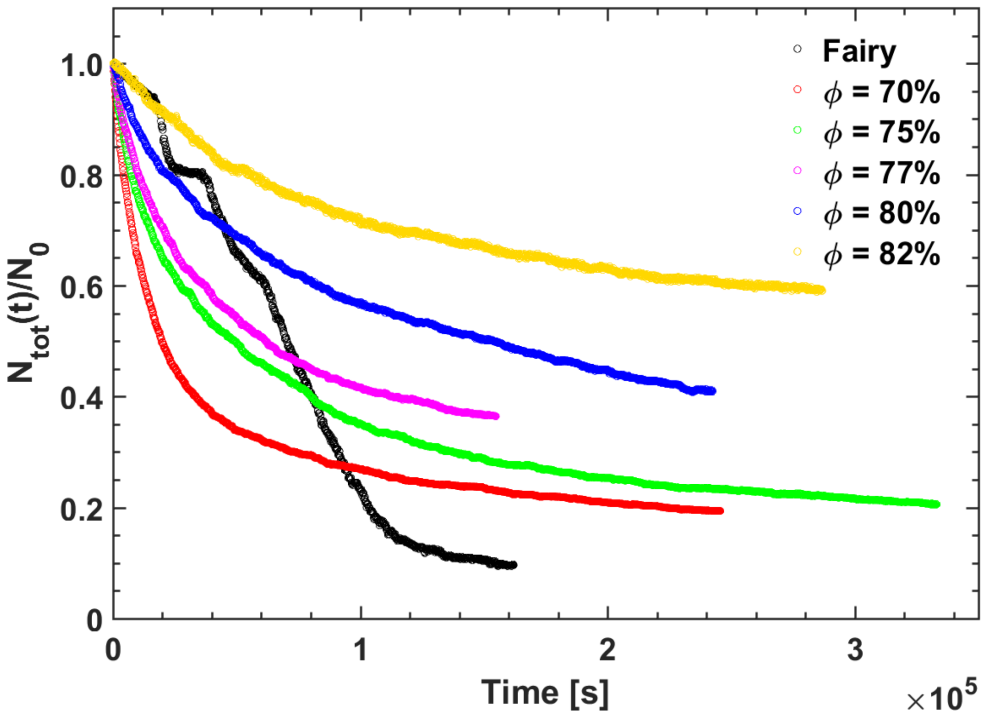

Figure 3.16: **Total number of bubbles.** *Total number of bubbles over time for foamed emulsions having different oil fractions. N_{tot} is normalised over the initial number of bubbles and the Fairy curve is reported to allow a visual comparison.*

We can see that the decrease of the total number of bubbles is smooth compared to what observed in Fairy foam. The steps observed in the Fairy curve corresponds to the approximately simultaneous disappearance of five-sided bubbles. But in the case of foamed emulsions, we start from a polydisperse 2D foam, hence the five-sided bubbles have different sizes and there is no reason why they should all disappear at the same instant. We can further observe that increasing the oil fraction the total number of bubbles decreases more slowly.

Thanks to the Matlab program, we can also get the evolution of the mean bubble area to see if these foamed emulsions exhibit a scaling behaviour. Once we have the mean area trend, we can easily find how the mean bubble size evolve over time.

It is unusual to find in the literature the evolution of the mean bubble radius over time for 2D foams, as the bubbles are usually not very small at the beginning in such experiments, so once they start ageing the statistics becomes poor quite soon. However, in our case we start with a polydisperse foam having very tiny bubbles and since the ageing results very slow, we can find out the trends of the mean bubble radii in order to compare them with the ones found for 3D foams.

By simply using the relation $\langle R \rangle = \sqrt{\langle A \rangle / \pi}$, we can plot the mean radius over time, after normalising it by its initial value R_0. What we find is reported in figure 3.17. Here we can observe that after a transient regime, for every foamed emulsion the mean bubble radius seems to exhibit an asymptotic power law evolution.

If we fit the final part of the curves with a function $\langle R \rangle / R_0 = a \cdot t^{\beta}$ we can estimate and compare the exponents for different oil fractions, which are reported in table 3.12.

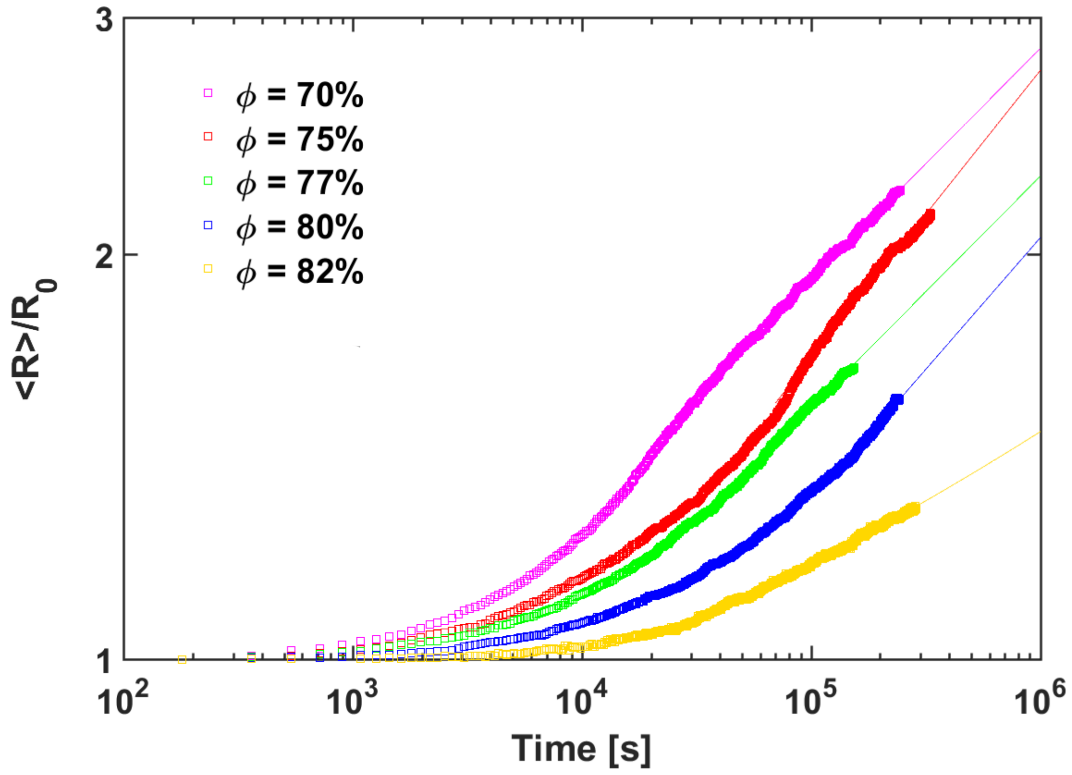

Figure 3.17: **Radius scaling.** *Normalised mean bubble radius over time at different oil fractions, obtained from the mean area scaling. The solid lines represent the fitting power laws* $\langle R \rangle / R_0 = a \cdot t^{\beta}$. *The exponents are reported in table 3.12.*

The exponent slightly varies for ϕ between 70% and 80%, while it is much smaller at ϕ=82%. We know from the literature that the prediction for dry foams is $\beta = 1/2$, whereas all the experimental exponents we obtained are smaller. They are all even smaller than the theoretical value $\beta = 1/3$ expected for the Ostwald ripening in wet foams. It is interesting to observe that, in contrast to 3D foams, 2D foams do not exhibit a plateau in the evolution of the mean bubble radius.

Radius scaling		
ϕ	a	β
70%	0.266 ± 0.001	0.172 ± 0.001
75%	0.143 ± 0.002	0.214 ± 0.001
77%	0.213 ± 0.002	0.172 ± 0.001
80%	0.138 ± 0.002	0.196 ± 0.001
82%	0.420 ± 0.001	0.090 ± 0.001

Table 3.12: **Scaling parameters.** *The table reports the parameters found by fitting the scaling curve of the normalised mean bubble radius for each 2D foamed emulsion. The curve used to interpolate is a function* $\langle R \rangle / R_0 = a \cdot t^{\beta}$. *The error associated to the parameters is the one coming from the interpolation and is probably underestimated.*

Conclusions

The aim of the present thesis was to investigate how the mechanical properties of the continuous medium impact on foam stability. More precisely, we wanted to probe the effect of the elasticity of the liquid phase on the coarsening process, in conditions of negligible drainage and coalescence.

For this reason, we chose to foam oil-in-water emulsions at high droplet concentrations, which exhibit viscoelastic properties suitable for our purposes. The choice of employing elastic emulsions to avoid gravitational drainage revealed itself successful, as foamed emulsions at high oil concentrations do not drain for very long periods of time. This feature provides foam samples suitable for carrying out experiments at constant liquid fraction, which is usually not possible on the ground because of gravity.

From the study of three dimensional foams, which were investigated through diffusing-wave spectroscopy, we observed a slowing down of the coarsening process for foamed emulsions having oil fractions higher than 70%. The growth of the mean bubble size has a peculiar behaviour, very different from traditional dry aqueous foams. After a transient regime where the bubbles grow, the mean bubble size seems to reach a saturation value, which is more evident at very high oil fractions. The photographs taken confirm this behaviour and clearly show that the higher the oil fraction in the liquid phase, the smaller the mean bubble size, considering the same time after foam creation.

We know from the literature that the gradual increase of elastic stresses among the bubbles can stabilise the entire foam [37], and that coarsening can halt if the yield stress of the continuous phase overcomes the Laplace pressure difference between bubbles [5] [23]. What we observed is that coarsening appears hindered when the Laplace pressure is overcome by the storage modulus of the emulsions, even if the yield stress is much lower.

The investigation of quasi-2D foams clearly revealed a strange evolution of the bubbles at such high oil fractions. We observed that gradually increasing the oil fraction from 70% to 82%, the monolayer of bubbles exhibits a surprising pattern, where bubbles are not at all relaxed. The material sample looks like the evolution of solid grains instead of gas bubbles.

From the image analysis we discover that the mean bubble size keeps on growing with an asymptotic behaviour described by a power law. This is in contrast with the plateau found for 3D foams. All the time exponents are smaller than the theoretical prediction of 1/2 for dry foams and even smaller than the value 1/3 expected for wet foams. Hence even in 2D foams a viscoelastic continous phase changes coarsening considerably.

The analysis of the film permeability revealed a low effective diffusion coefficient. Since this coefficient depends on several parameters, many hypotesis can be made for justifying the result obtained. However, the lack of studies in similar systems does not allow to derive a full explanation of what we observed and further experiments are required to pinpoint the origin of the slow diffusion.

The point of interest we can highlight is that changing the elastic properties of the emulsions does influence the coarsening process, and this partially answers to the initial question of this work. What we have seen is that the elastic continous phase leads to a slower coarsening, and can even stop the process. However, we still do not have a complete picture of how the coarsening process is modified by the presence of the oil droplets inside the foam.

This change in coarsening mechanism gives rise to many open questions. Recent studies [3] suggest that one should consider the yield stress of the total foam, not the one of the continuous phase. Then, rheological tests on foamed emulsions could probably help to understand more about the coarsening mechanism in such systems.

An in-depth analysis of the autocorrelation functions, obtained from spectroscopy, can give relevant information about the structural rearrangements inside the foam: as foamed emulsions contain two types of scatterers, one needs to find a way to decouple the contributions of bubble rearrangements from the ones of droplets dispersed in the liquid phase. However, this would allow us to probe how the bubble rearrangements evolve during the coarsening process and whether an arrest of the coarsening is indeed observed through an arrest in rearrangements.

Furthermore, it would be interesting to understand whether the thin films effectively contain oil droplets at the interfaces or not, as this can also change the film permeability.

We can conclude that the results obtained in this study are quite satisfying, as they lay the groundwork for many further experimental investigations.

Bibliography

[1] R. Battino, T. R. Rettich, and T. Tominaga. **The Solubility of Nitrogen and Air in Liquids.** *Journal of Physical and Chemical Reference Data*, 1984.

[2] V. Bergeron. **Forces and structure in thin liquid soap films.** *J. Phys.: Condensed Matter*, 11:215–238, 1999.

[3] H. Bey, F. Wintzenrieth, O. Ronsin, R. Hohler, and S. Cohen-Addad. **Stabilization of foams by the combined effects of an insoluble gas species and gelation.** *Soft Matter*, 13:6816–6830, 2017.

[4] J. Bibette, F. Leal-Calderon, V. Schmitt, and P. Poulin. ***Emulsion Science: basic principles, an overview.*** Springer Tracts in Modern Physics, 2002.

[5] Z. Briceno-Ahumada, A. Soltero, A. Maldonado, J. Perez, D. Langevin, and M. Impéror-Clerc. **On the use of shear rheology to formulate stable foams. Example of a lyotropic lamellar phase.** *Colloids and Surfaces A: Physicochemical and Engineering Aspects*, 507:110–117, 2016.

[6] I. Cantat, S. Cohen-Addad, F. Elias, F. Graner, R. Hohler, O. Pitois, F. Rouyer, and A. Saint-Jalmes. ***Foams. Structure and Dynamics.*** Oxford University Press, New York, 2013.

[7] E. M. Cuvelier, P. Soto, F. Courtois, B. Broyart, and C. Bonazzi. **Oxygen solubility measured in aqueous or oily media by a method using a non-invasive sensor.** *Food control*, 73:1466–1473, 2017.

[8] R. Deleurence, T. Saison, F. Lequeux, and C. Monteux. **Time scales for drainage and imbibition in gellified foams: application to decontamination processes.** *Soft Matter*, 11:7032–7037, 2015.

[9] E. Dickinson. ***Food Emulsions and Foams***. Woodhead Publishing Limited, England, 1986.

[10] W. Drenckhan and A. Saint-Jalmes. **The science of foaming.** *Advances in Colloid and Interface Science*, 2015.

[11] D. J. Durian, D. A. Weitz, and D. J. Pine. **Multiple Light-Scattering Probes of Foam Structure and Dynamics.** *Science*, 252:686–688, 1991.

[12] D. J. Durian, D. A. Weitz, and D. J. Pine. **Scaling behavior in shaving cream.** *The American Physical Society*, 44, 1991. Physical Review A.

[13] B. Esteban, J. R. Riba, G. Baquero, R. Puig, and A. Rius. **Characterization of the surface tension of vegetable oils to be used as fuel in diesel engines.** *Elsevier: Fuel*, 102:231–238, 2012.

[14] E. Forel. **Mûrissement et coalescence de mousses liquides.** PhD thesis. Matériaux. Université Paris-Saclay, 2017. Français.

[15] T. Gaillard, M. Roché, C. Honorez, M. Jumeau, A. Balan, C. Jedrzejczyk, and W. Drenckhan. **Controlled foam generation using cyclic diphasic flows through a constriction.** *International Journal of Multiphase Flow*, 96:173–187, 2017.

[16] R. M. Guillermic, A. Salonen, J. Emile, and A. Saint-Jalmes. **Effect of Bulk and Interfacial Rheological Properties on Bubble Dissolution.** *Journal of Colloid and Interface Science*, 237:158–166, 2001.

[17] R. M. Guillermic, A. Salonen, J. Emile, and A. Saint-Jalmes. **Surfactant foams doped with laponite: unusual behaviors induced by aging and confinement.** *Soft Matter*, 5:4975–4982, 2009.

[18] S. Hilgenfeldt, S. Arif, and J. C. Tsai. **Foam: a multiphase system with many facets.** *Phil. Trans. R. Soc.*, 366:2145–2159, 2008.

[19] R. Hohler and S. Cohen-Addad. **Rheology of liquid foam.** *J. Phys.: Condensed Matter*, 17:1041–1069, 2005.

[20] P. D. Kaplan, A. D. Dinsmore, A. G. Yodh, and D. J. Pine. **Diffuse-transmission spectroscopy: A structural probe of opaque colloidal mixtures.** *Physical review E*, 50:4827–4835, 1994.

[21] S. A. Koehler, S. Hilgenfeldt, and H. Stone. **A generalized view of foam drainage: experiment and theory.** *Langmuir*, 16:6327–6341, 2014.

[22] R. G. Larson. ***The structure and rheology of complex fluids.*** Oxford University Press, New York, 1999.

[23] I. Lesov, S. Tcholakova, and N. Denkov. **Factors controlling the formation and stability of foams used as precursors of porous materials.** *Journal of Colloid and Interface Science*, 426:9–21, 2014.

[24] T. G. Mason, J. Bibette, and D. A. Weitz. **Elasticity of compressed emulsions.** *Physical review letters*, 75:2051–2054, 1995.

[25] T. G. Mezger. ***The Rheology Handbook.*** Vincentz Network, Hanover, Germany, 2014.

[26] W. W. Mullins. **The statistical self-similarity hypothesis in grain-growth and particle coarsening.** *Journal of Applied Physics*, 59:1341–1349, 1986.

[27] W. W. Mullins. **Estimation of the geometrical rate-constant in idealized 3 dimensional grain-growth.** *Acta Metallurgica*, 37:2979–2984, 1989.

[28] D. J. Pine, D. A. Weitz, J. X. Zhu, and E. Herbolzheimer. **Diffusing-Wave spectroscopy: dynamic light scattering in the multiple scattering limit.** *J. Phys. France*, 51:2101–2127, 1990.

[29] N. Politova, S. Tcholakova, Z. Valkova, K. Golemanov, and N. D. Denkov. **Self-regulation of foam volume and bubble size during foaming via shear mixing.** *Colloids and Surfaces*, 539:18–28, 2018.

[30] E. Rio and A. L. Bianche. **Thermodynamic and Mechanical Timescales Involved in Foam Film Rupture and Liquid Foam Coalescence.** *ChemPhysChem*, 15:3692–3707, 2014.

[31] R. Sander. **"Henry's Law Constants".** *in NIST Chemistry WebBook, NIST Standard Reference Database.*

[32] L. Saulnier. **Étude de la coalescence et du mûrissement dans les mousses liquides : des expériences modèles à différentes échelles.** PhD thesis. Université Paris-Sud, 2012. Français.

[33] M. Schneider. **Stabilité et rhéologie des mousses d'émulsions attractives.** PhD thesis. Université Paris-Sud, 2018. Français.

[34] L. L. Schramm. ***Emulsions, Foams and Suspensions. Fundamentals and Applications.*** Wiley-VCH, Weinheim, 2005.

[35] S. Tcholakova, Z. Mitrinova, K. Golemanov, N. D. Denkov, M. Vethamuthu, and K. P. Ananthapadmanabhan. **Control of ostwald ripening by using surfactants with high surface modulus.** *Langmuir*, 27:14807–14819, 2011.

[36] M. U. Vera, A. Saint-Jalmes, and D. J. Durian. **Scattering optics of foam.** *Applied Optics*, 40, 2001.

[37] A. J. Webster and M. E. Cates. **Osmotic Stabilization of Concentrated Emulsions and Foams.** *Langmuir*, 17:595–608, 2001.

[38] D. A. Weitz, J. X. Zhu, D. J. Durian, H. Gang, and D. J. Pine. **Diffusing-Wave Spectroscopy: The Technique and Some Applications.** *Physica Scripta*, T49:610–621, 1993.